LSTN Perovskite/Graphite Carbon Nitride Hybrids as Electro Catalyst for Water Splitting.

By

Umair Ali Asif

School of Chemical and Materials Engineering

National University of Sciences and Technology

2022

LSTN perovskite/Graphite Carbon Nitride Hybrids as Electro Catalyst for Water Splitting.

Name: Umair Ali Asif

Reg no: 00000327658

This thesis is submitted as a partial fulfilment of the requirements for

The degree of

MS in Chemical Engineering

Supervisor Name: Dr. Tayyaba Noor

School of Chemical and Materials Engineering (SCME)

National University of Science and Technology (NUST)

H-12, Islamabad, Pakistan

2022

Dedication

By the grace of Almighty Allah, who is the most Beneficent and the most merciful
this research is dedicated to my parents, who have always been my source of guidance and support.
To my supervisor who shared her knowledge, gave advice, and encouraged me to fulfil my tasks.
To all my fellows, with whom I worked with and shared good memories and to the seekers, willing to do some things in their lives.

Acknowledgment

All praises to **Almighty Allah**, without His will nothing can happen, who favoured us with the capacity to think and made us anxious to investigate this entire universe. Incalculable greetings upon the **Holy Prophet Hazrat Muhammad (PBUH)**, the reason for the creation of the universe and wellspring of information and blessing for whole humankind.

From the core of my heart, I am thankful to my research supervisor, **Dr. Tayyaba Noor** for her unwavering technical and moral support and enlightening me with a research vision and pushing me for excellence. Her quest for perfection and excellence had been a source of inspiration and driving force. It is her consistent and encouragement that empowered me to achieve the onerous milestone.

I extend my sincere gratitude towards my co supervisor guidance and committee members: **Dr. Erum pervaiz, Dr. Amin Shahid and Dr. Muhammad Aftab Akram** for guiding and supporting me in my research course. It would not have been possible without them. I express my gratitude for Dr. Tayyaba Noor for letting me work in Chemistry Lab.

My Seniors **Neelam Zaman and Sadia Altaf** shared their knowledge regarding catalysis and Catalyst's synthesis techniques, and they were the motivation for me in this entire research work. Without any doubt, SCME's supporting staff coordinated with me while I was working on different equipment especially in Heat treatment lab, Chemical synthesis lab, Chemistry lab etc. I am highly obligated to my Parents and siblings for their never-ending love. Thanks for believing in me, wanting the best for me, and inspiring me to follow my passion. To my friends, thank you for your support, advice and encouragement.

Umair Ali Asif

Table of Contents

List of Abbreviations

OER: Oxygen Evolution Reaction

ORR: Oxygen Reduction Reaction

HER: Hydrogen Evolution Reaction

G-CN: Graphitic carbon nitride

ECSA: Electrochemically active surface area

SEM: Scanning electron microscope

FTIR: Fourier Transform Infrared Spectroscopy

CV: Cyclic Voltammetry

LSV: Linear Sweep Voltammetry

EIS: Electrochemical Impedance Spectroscopy

EDS: Energy-dispersive X-ray spectroscopy

NF: Nickel Foam

Sr: Strontium:

La: Lanthanum:

Ti: Titanium:

O_x: Oxidation:

O_2: Oxygen:

Fe: Iron

Cr: Chromium

Cu: Copper

Pt: Platinum

Red: Reduction

List of Figures

List of Tables

Abstract

For future energy uses and transportation, the electrochemical splitting of water utilizing renewable energy is being explored as a sustainable and environmental friendly source of hydrogen fuel. Even so, the mass production through water splitting is restricted due to lower stability of the electrode materials, the successful development of the HER phase in acidic conditions, along with the sluggish kinetics and higher values of overpotential of the complicated OER process involving four electron transfers. These factors combine to make the process difficult. As a result, one of the primary goals of the ongoing study is to develop an efficient bi - functional electrocatalyst that can minimize the overpotential for both OER and HER.

The development of highly effective bi - functional electrocatalysts for use in water splitting reactions had been the main focus of this research. The primary emphasis has been done on the preparation of perovskite materials and its hybrids with other active materials. They have a tune able electronic structure due to the compositional and crystalline malleability of perovskite oxides. Herein, LSTN perovskite has been synthesized initially followed by its exsolution in a reduced environment. The hybrid of LSTN has been made with a g-C_3N_4, to develop LSTN@g-C_3N_4 coated on very conductive nickel foam. Currently, research has been driven towards double perovskite due to the stable nature of non-stoichiometric perovskite that has an immense influence on transition metal 3d σ*- antibonding (eg) orbital electron filling. Moreover, the catalysts have been characterized by x-ray diffraction (XRD), Fourier transform infrared spectroscopy (FTIR), Raman spectroscopy, energy dispersive x-ray spectroscopy (EDX), and Scanning electron microscopy (SEM). The results of these characterization represents that catalysts have been prepared successfully. The bifunctional activity of catalysts has been tested by calculating Tafel slope, overpotential, and mass activity. Among the prepared hybrids, 3 wt. % LSTN@g-C_3N_4, has shown the most proficient results with high stability and low resistance value.

Chapter No 1

Introduction

An energy system which is sustainable as well as eco-friendly and with least consumption of natural sources is one of the pivotal targets of scientist for future [1, 2]. In year 2013, the world's energy demand was 18 TW; data shows that 80% of that came from natural sources (coal, oil and gas) [3]. The increase in global energy demand is anticipated to be 23 or 25 TW up till year 2040, followed by the scenario of “recent policies” accordingly. Also, the increase in carbon dioxide emissions is predicted to be 37 or 44 Gt yr^{-1} in 2040, which was recorded to be 32 Gt yr^{-1} in 2013. And all this is to happen because of the rapid population growth and increased industrialization. The situation seems quite alarming because of the increase in energy demand and supply and a drastic decrease in the sources responsible for its production. For the purpose of nature and climate preservation, the world is focusing its attention and resources on developing energy systems that utilise sustainable form of energy (hydroelectric power, solar power, and wind power)[4].

An increase in the production and usage of renewable resources in electricity sector is pivotal, from the figures of 2010 it was only 2.1 TW out of 17.6 TW which is 12 % of the global energy demand[5]. The increased penetration of renewable resources is also required in transportation and chemical industry which was 19 % in 2010, i.e., 3.3 TW out of 17.6 TW, where 43% (1.4TW) of it was by light duty vehicles and the rest 57 % (1.9 TW) was consumed by heavy duty vehicles, rail, aviation and marine. Among the consumption by light duty vehicles electrification (electric cars) is already decarbonizing the environment but electrification in heavy duty vehicles is quite difficult[5]. As a result, it is anticipated that among light duty vehicles the energy demand will remain the same or even decrease but the consumption of energy by commercial transportation will rise by approximately 2/3 from 2010 to 2040, which is 1.9 to 3.2 TW. In the same way the energy demand in chemical industry is currently 8 % of global energy which is (1.5 TW) which is likely to grow by 2/3 from 2010 to 2040 which is 1.5 TW to 2.5 TW as the worldwide demand of plastic and fertilizer will increase[5]. Owing to all these circumstances the world is focusing on the production of chemical fuels which are sustainable and are a much more natural and

cheap resource of energy. For this the industrial chemicals like, CH_3OH (40×10^6 Ton per year), C_2H_4 (116×10^6 Ton per year), C_3H_6 (74×10^6 Ton per year), H_2 (50×10^6 Ton per year), H_2O_2 (2.2×10^6 Ton per year), NH_3 (175×10^6 Ton per year) etc., could be used as a reliable energy resource for the generation of chemicals to make products needed worldwide on daily basis with reduced emission of CO_2 [6]. The **Fig.** 1 illustrates the renewable sources for production of energy.

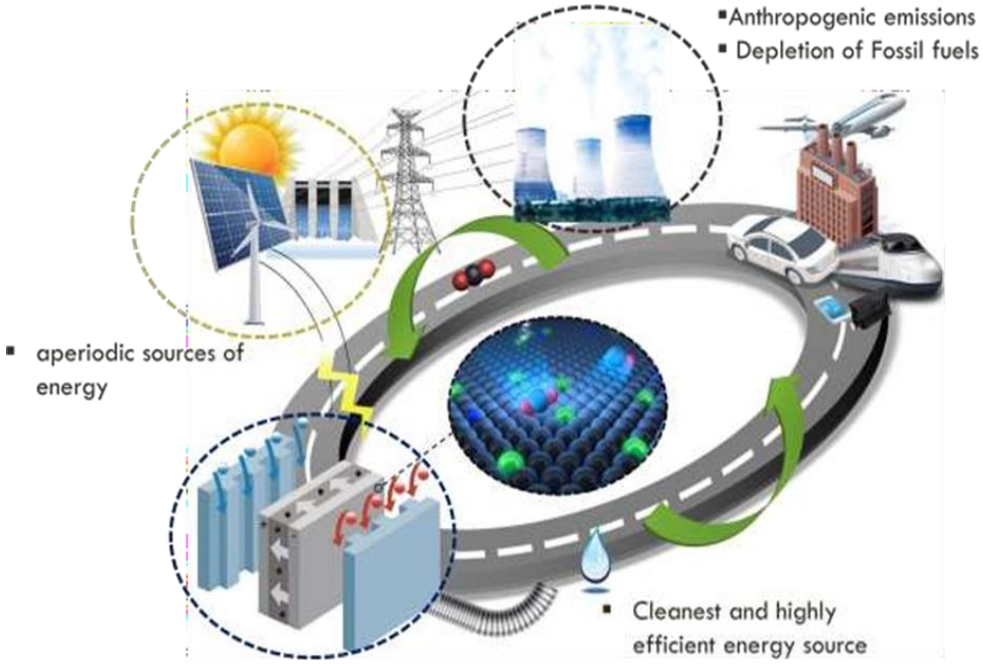

Figure 1: *Schematic illustration of resources that can be used for generating energy to perform water splitting.*

The Earth's atmosphere contains CO_2, nitrogen and water which can be used for the production of hydrocarbons, ammonia and oxygenates. Electrochemical techniques for renewable energy can then be utilised to produce vital fuels and chemicals, but only if catalysts with the appropriate characteristics can be produced. For example, for a sustainable source of hydrogen, water splitting reaction (OER & HER) is of great scope [7, 8]. In fuel cells, hydrogen is oxidised and oxygen is reduced, which results in the transformation of chemical energy into electrical energy. Hydrogen peroxide that is used in water treatment industries as well as in the bleaching of pulp and paper can also be gained from oxidation reduction reactions. This is one of the many uses for the stable hydrogen that is produced as a by-product of this process. In the same way, CO_2 in the atmosphere or coming from other sources can be used for the production of certain fuels, chemicals, polymers and plastics by preliminary electro

reduction [3]. Similarly, nitrogen going through electrochemical process produces ammonia which is used for fertilizer production, and also on their application in a required concentration, also in Haber Bosch process and in the prevention of environmental hazards in case of run off. Given to all these uses of these natural resources an efficient and improved electrocatalysts with selective abilities for specific transformations is crucial[4].

For an enhanced electro catalytic system two main methods are used

- By providing more active sites on given electrode
- Improving the level of activity that is already there at each active site

The respective ways are mutually exclusive and in an ideal case can be addressed simultaneously, thus giving the utmost improvement. But there are limitations to them as well such as, the maximum amount of charge that can be loaded on the electrode leaving the processes such as charge and mass transport unaffected.

Electrocatalytic water splitting is an ideal technique for the generation of oxygen and hydrogen, which can be used in various applications. [9, 10]. The most important step of the water-splitting process, also called the oxygen evolution reaction, is the formation of an O-O bond and four proton-coupled electron transfers. This is a very slow process that delays, so a catalyst is needed (OER) [11-13]. Until now, inert metals or oxides such as RuO_2 or IrO_2 are claimed to be "state-of-the-art" electrocatalysts during oxygen evolution process (OER). However, the fact that these electrocatalysts are both expensive and rare acts as a barrier to their production on a wide scale.[14, 15]. They are also susceptible to oxidation with alkaline electrolytes due to the fact that they are unstable metals. Because of these factors, a great deal of effort and study are currently being put into the investigation of many options that have advantages such as affordable cost, abundance on earth, highly efficient, and stable.[16, 17].

The process in which water break down into hydrogen and oxygen is known as water splitting Based on the source of power water splitting is divided into three types; electrochemical, photochemical and thermochemical water splitting. When electrical energy is used to breakdown water then it is called electrochemical water splitting. For the production of hydrogen on a large scale from water splitting reactions, significant efforts are necessary to create electrocatalysts that are both catalytically active and economically viable Numerous earth-abundant cost effective materials such as metal

phosphides, carbides[18] transition metal oxides[19] (e.g., perovskites and spinel oxides), carbonaceous materials, [20] transition metal dichalcogenides[21-23], and selenides[24] have been intensively researched for OER in recent years. However, the utilization of most cheap metal catalysts is still challenging for HER as a catalyst showing higher activity for OER may not be active for HER. Therefore, a bifunctional electrolysis cell does not fulfil the electro catalytic efficiency requirements for the total water splitting process. So, these difficulties need the development of a stable bifunctional electro catalyst which is equally active for OER and HER reactions.

1.1 Transition Metal Oxides

Graphitic carbon nitride, also known as g-C_3N_4, is a material that is considered to be among the most desirable due to its exceptional electrochemical properties [25]. In addition, g-C_3N_4 is capable of performing the function of an electro catalyst for both OER and HER; however, the applicability of g-C_3N_4-based materials is hampered by their low conductivity and limited availability of redox sites. [26]. Therefore, in order to eliminate the constraints of g-C_3N_4, numerous approaches have been taken. One of these strategies is composite synthesis containing high conductivity and active elements. However, the findings are still a long way from a practicable implementation of the use of g-C_3N_4 in water splitting. Hybrid materials, on the other hand, with increased conductivity and the ability to make surface redox active spots more readily accessible, could make this a reality[27]. So g-C_3N_4 is pinned with LSTN perovskite to increase the activity. The problem associated with conductivity of catalysts can be resolved by directly growing metal oxides over Ni foam that provide high surface area [28]. The hybrid nanostructure is able to reduce the overpotential and improve the current density for both halves of the reaction because it makes use of the benefits offered by both of its constituent parts.

Because they are inexpensive and allow for the bonds of oxygen species, TMOs have the potential to perform the same function as the more conventional precious metal oxygen electro catalyst. Perovskites are thought to be preferable because they have an excellent capacity to accommodate a wide variety of cations, and they also have the ability to facilitate partial cationic substitution at both the A-site and the B-site. The partial replacement serves a variety of objectives including producing an oxygen vacancy and generating various valance states in the cations that are located at the A/B site. Perovskite oxides are able to boost catalytic activity by controlling the adsorption

mechanism of reaction intermediates. This is accomplished through the appropriate compositional changes and the electrochemical stability of the perovskite oxides[29, 30]. Perovskites are said to have a formula of ABO_3, in which the A-site is occupied by rare-earth metals and the B-site is occupied by transition metals. This denotes basic and realistic values due to the compositional and structural variability of perovskite based catalysts, as well as their magnetic and ionic characteristics, distinctive electronic framework, inexpensive, and chemical durability. [31-34] . In spite of their enhanced activity, its low conductivity, that enhances the resistance to charge transfer as well as their long-term durability, is a concern which needs to be tackled in order to attain high efficiency. [15, 35].

1.2 Mechanism on the Catalyst Surface

1.2.1 Electrochemistry of Water Splitting

The catalyst is applied on anode and cathode where it assists in carrying out OER and HERs, by speeding up the water splitting mechanism [36]. The reaction can occur in an alkaline media or an acidic media with the given mechanism as follows [37, 38].

In acidic solution

At cathode

$$2H^+ = 2e^- \rightarrow H_2 \quad (1)$$

At anode

$$H_2O \rightarrow 2H^+ + \tfrac{1}{2} O_2 + 2e^- \quad (2)$$

In neutral or alkaline solution

At cathode

$$2H_2O + 2e^- \rightarrow 2OH^- \quad (3)$$

At anode

$$2OH^- \rightarrow H_2O + \tfrac{1}{2} O_2 + 2e^- \quad (4)$$

Alkaline electrolytes, in comparison with acidic electrolytes, allow precious metal catalysts such as platinum, Iridium, or ruthenium, to be substituted with cheap metals or catalysts having carbon as functional group. [39]. As represents in **Fig. 2**.

Figure 2: *Schematic overview of different perovskite catalyst used for water Splitting reaction of HER and OER*

1.2.2 Hydrogen Evolution Reaction Mechanism

The HER as a whole functions at the established potential of -829 mV while operating in alkaline conditions. In general, the HER process consists of three steps, each of which is processed by three different kinds of eight reactions, Eq. 5-9 in both acidic and alkaline phase respectively[37]. These reactions are specified below: [40, 41].

Volmer reaction (adsorption electrochemically) (Eq. 5-6)

$H^+ + * + e^- \rightarrow H^*$ (In acidic medium)

(5)

$H_2O + * + e^- \rightarrow H^* + OH^-$ (In alkaline medium)

(6)

Heyrovsky reaction (desorption electrochemically) (Eq. 7-8)

$H^* + H^+ + e^- \rightarrow * + H^2$ (In acidic medium) (7)

$H^* + H_2O + e^- \rightarrow * + H_2 + OH^-$ (In alkaline medium) (8)

Tafel reaction represented in eqn. 9

$$2H^* \rightarrow 2 * + H_2 \quad (9)$$

Volmer reaction pathways are involved in Heyrovsky and Tafel steps that involves the molecular adsorption of H_2O molecules over the bared active sites. Electro-chemical reduction of the H_20 molecule adsorbed on the active site at $H*$ and OH leads to adsorption of OH and the release of the H_2 molecule from the surface. A mechanism was suggested for perovskite oxide catalyst exhibits that perovskite oxide own non-metal reactive site, rather a surface charged oxygen that is negatively charged serves the purpose. A mechanism showing alkaline HER steps, given in **Fig. 3**, was suggested by Xu et al.[42]. The efficiency of $Pr_{0.5}$ $(Ba_{0.5}Sr_{0.5})_{0.5}Co_{0.8}Fe_{0.2}$ $O_{3-\delta}$ perovskite oxide in catalysing HER is discussed. The mechanism presents that the water molecule available from electron and electrolyte, that interaction with an active site occupied by oxygen to evolve as an intermediate given as adsorbed H^*, where, the metal sites in vicinity either gets or decreases (having state of oxidation toggle between n+1 and n). Though, the involvement of second step (Heyrovsky reaction or Tafel reaction) is not easy to guess, various reaction intermediaries are obtained in OER/ORR. But, there is only one intermediate achieved during the two electron transfer HER, this thus, provides zero over potential for highly active catalysts (e.g., Pt)[43] which shows a need to improve perovskite catalysts. HER rate depends on binding capability of H* intermediate, that is generally given free energy for hydrogen adsorption (ΔGH)[44]. The efficiency of HER catalyst depends upon its binding ability of hydrogen, which should be in between strong and week, providing a ΔGH value close to zero[35].

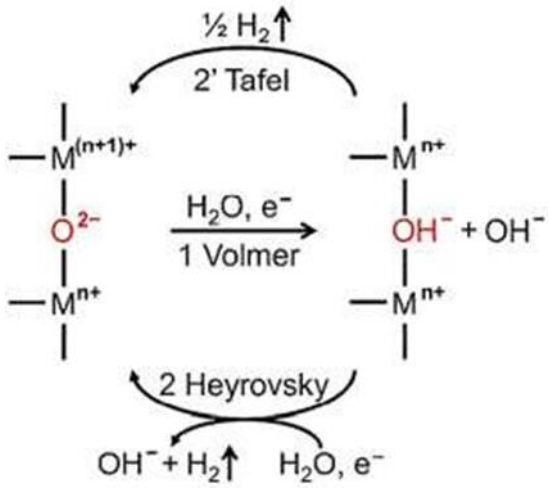

Figure3: *Proposed mechanism for HER at the surfaces of perovskite oxide*

1.2.3 OER/ORR Reaction Mechanism

1n 1977, Tseung and Jasem [41] suggested that new active sites are generated at higher oxidation states when transition metals are attached with an oxidative electrode at lower current than that of the electrode containing oxygen. This was based on the observation that higher oxidation states correspond to higher levels of activity. From 1980 to 1984, Trasatti[45, 46] conducted research using perovskite-type oxides and discovered a volcano-type link between OER over potential and enthalpy of phase transition from less state of oxidation to a high state of oxidation. When tested at a constant over potential, Bockris and Otagawa [47, 48] investigated eighteen different perovskite oxides and realise that current density and enthalpy of formation is inversely proportional at same over potential.

In this study Man et al.[49] Came to the conclusion that the scope of the mechanism that was previously given may be expanded. The mechanism shown in Figure 4(b) is composed of a channel of different acid-base stages, one of which involves the oxygen hydroxyl (OH-), which aims for a Lewis base that is an electron acceptor for metals only [41]. The equation for the ORR mechanism using alkaline media is $O_2 + 2H_2O + 4e^- \rightarrow 4OH^-$ [38], using an established electrode potential of 401mV. A four-step process is accountable for the reaction that takes place at metal sites[50]. As indicated in Figure 4(c), the sequence of reactions is as follows: 1). Hydroxide replacement; 2). Formation of Peroxide; 3). Formation of oxide; and 4). Regeneration of hydroxide. The initial step includes Water or molecular oxygen and an electron, which combines with surface of metal sites to form compounds containing oxygen represented as OO*, OOH*, O*, and OH*, where * denotes a reacting site on the surface of catalyst. Such oxygenated adsorbates, the state of oxidation which can switch between n+ and n+1, are accompanied by oxidation and reduction (redox) processes that occur at surface of metal active sites. Amount of energy that O_2 may bind to and surface metal sites are two major factors that influence the rate of the oxygen reduction process (ORR). When the binding energy of oxygen is low, the shifting of OH* to OO* is known to by the rate determining step (RDS), but when the binding energy of oxygen is high, the final step from O* transition to OH* is directed as the rate limiting step (RLS). In accordance with the Sabatier principle, the ideal perovskite catalyst will have a moderate amount of oxygen binding energy[50, 51]. According to Suntivich et al. [52] e_g orbital filling in metal cations has a significant

impact on the step which determine rate. They proposed if the value e_g was more than one then the production of an oxygen to oxygen single bond in an OOH* adsorbate could really asses the rate. This was stated in their study. The generation of O-O ion from oxy-hydroxide could be a rate-determining step (RDS) for numbers less than one. A similar method could be observed for OER in **Fig. 4** which involves the regeneration of OH- and its subsequent disappearance. For OER, the surface response of perovskite in an alkaline medium can be expressed as $4OH^- \rightarrow O_2 + 4e^- + 2H_2O$, which proceeds through four distinct steps which are listed as follows: 1) Hydroxide deprotonation; 2) Peroxide formation; 3) Peroxide deprotonation; and 4) Hydroxide formation (Fig. 4(d)). In the following mechanism, OH- derived from the electrolyte reacts with the metal sites that are performing redox reaction on metallic surface as the state of oxidation switches among n^+ and n^{+1}. O*, OO*, OH*, and OOH* are the order in which the reactive intermediates appear in this sequence. The degree to which oxygen is able to attach to metal sites is another factor that determines the rate at which OER reactions proceed. The generation of peroxide (O* to OOH*) represents the rate-limiting step (RLS), which occurs when oxygen binds in an insufficiently strong manner. While in the phase of deprotonation, wherein O_2 attaches very tightly, it functions as a step that determines the rate of the reaction (RDS))[52]. Due to scaling , relations, and estimating the nonzero over potential for several known perovskites, The energy that binds oxygen adsorbate at the surface of OER and ORR is highly interdependent[49].

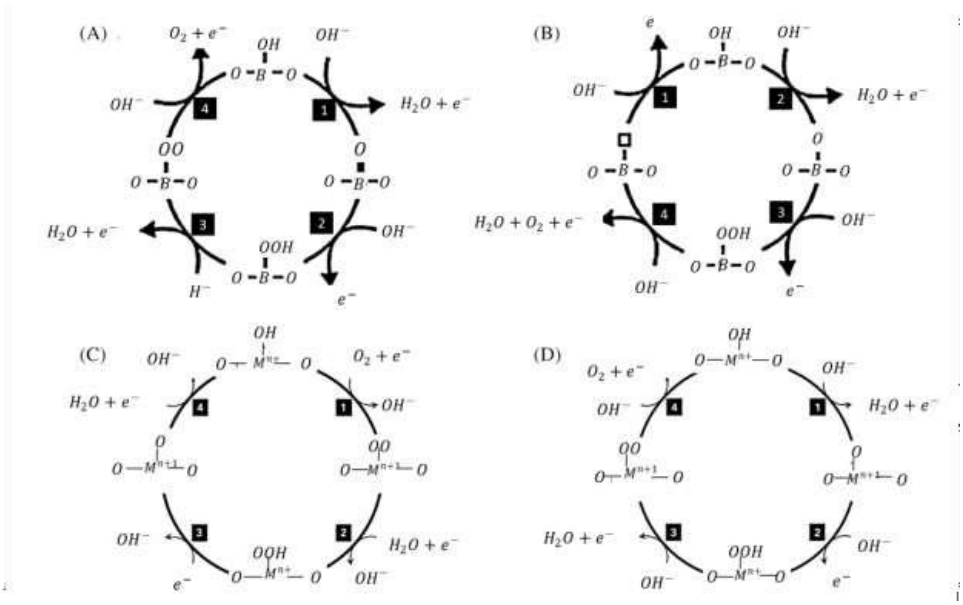

Figure 4: *OER/ORR scheme suggested for the surfaces of oxides*

OER/ORR scheme suggested for oxide surfaces59. a) The ORR on perovskite surfaces follows a suggested process with a total of four steps that was developed by Goodenough et al. b) A suggested reaction mechanism with four stages, C) ORR scheme for the perovskite that involves four electrons (d) OER mechanism with 4 electrons at surface of perovskite in alkaline media [39, 49, 50, 52]

In the ORR and OER reactions described above, the assessments based on density functional theory (DFT) suggest the existence of a variety of intermediates on the surfaces of perovskite oxide. In spite of the fact that the estimated elementary steps are very similar to one another, the sequence in which the intermediates appear is O_2^*, OOH*, O*, and OH* for ORR.[53], However, the order of the intermediates for OER is OH*, O*, OOH*, and O_2^* on metal sites [54]. The difference can be attributed to the fact that the surface characteristics of metals and perovskite oxides can vary greatly from one another. As demonstrated in Equation 6-9, the scaling relation can be used to determine the relationship among the adsorption energies of oxygen-binding species that are involved in the reaction mechanism [49],[55]. The difference in theoretical over potential among two oxide surfaces can be defined by a single descriptor. This descriptor could be both the adsorption energy of oxygen (ΔG_o) and the relative stability of OH^* vs OOH^* (ΔG_{OH} - ΔG_{OOH}). Both of these descriptors are given [55],[49]. As a consequence of this, a relation in the shape of a volcano was generated by applying Sabatier's principle. This connection places $LaNiO_3$ and $SrCoO_3$ close to the top of the chart as a result of their low over potential, which was achieved as a result of optimal oxygen binding. $LaCoO_3$, $LaFeO_3$, $LaMnO_3$, $LaCrO_3$, and $LaVO_3$ are located on the left hand of the volcano because to the high oxygen bonding they have. On contrary, $LaCuO_3$ is found the key element of the volcano due to poor oxygen binding.

$$* + H_2O \rightarrow OH^* + e^- + H^+ \quad (10)$$

$$OH^* \rightarrow O^* + e^- + H^+ \quad (11)$$

$$O^* + H_2O \rightarrow OOH^* + e^- + H^+ \quad (12)$$

$$OOH^* \rightarrow O_2 + e^- + H^+ \quad (13)$$

Since the subsequent investigations do not correspond to the previously proposed process, they are unable to explain the recent results of experiments depends on coated

TMOs like BSCF and LSTN [56]. current DFT simulations by Mefford et al.[57] explains that the participation of lattice oxygen in the OER reaction could be used to explain the high activity of catalyst of $La_{1-x}Sr_xO_{3-\&}$ and related compounds. Additionally, a recent work using DFT assessments revealed the novel OER schemes (Eq. 10-13), wherein single oxygen participates by creating reversible surface oxygen vacancies (V_o) [58]. $LaNiO_3$ shows the movement of oxygen vacancies on the surface towards the plane is exceptionally good then other perovskites, and this is necessary in order to react with OH* to generate Vo and OO*.

$$OH^* \rightarrow (V_o + OO^*) + H^+ + e^- \quad (14)$$

$$(V_o + OO^*) + H_2O \rightarrow O_2 + (V_o + OH^*) + H^+ + e^- \quad (15)$$

$$(V_0 + OH^*) + H_2O \rightarrow (H^*_{0-site} + OH^*) + H^+ + e^- \quad (16)$$

$$(H^*_{0-site} + OH^*) \rightarrow OH^* + H^+ + e^- \quad (17)$$

Therefore, the adsorbate evolution mechanism (AEM), which is shown in Eq. 6-9[49, 55] is one of the two suggested mechanisms for OER and The lattice-oxygen participation mechanism (LOM), which is shown in equations Eq. (14-17 can play a role in developing extremely active perovskites. The potential preferable mechanism for each separate perovskite is illustrated in **Fig. 5** and can be either an AEM or LOM.

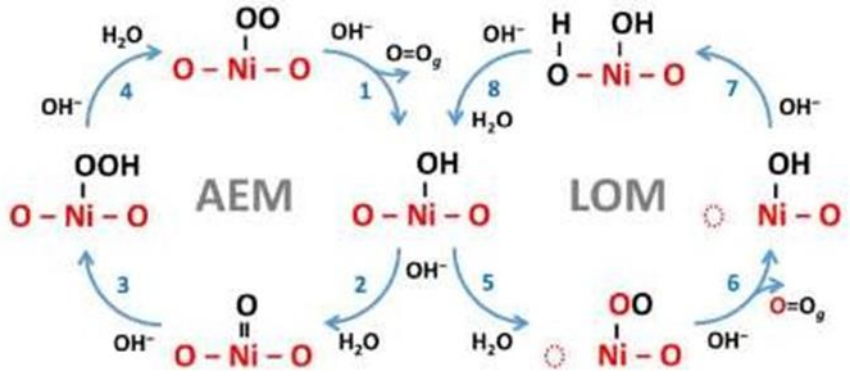

Figure 5 *Representation of the adsorbate evolution mechanisms and the lattice-oxygen participation mechanisms*

Chapter No 2

Literature Review

Perovskite based catalysts were regarded a better option for research beginning in the late 1990s, when scientists shifted their focus toward more cost-effective sources of accelerating such reactions. At that time, perovskites were deemed a good alternative. In a practical situation, increasing the efficiency of a perovskite based electro catalyst could be accomplished in two different methods. One strategy is to try to maximise the natural increase in activity at each reactive site by taking into account the physicochemical characteristics of the perovskite based catalyst's electronic frameworks. The characteristics contains a broad diversity of composition, which was accomplished through several processes like as substitution, oxygen vacancy, and the formation of a variety of crystal forms. Looking for another method which helps to increase reactive sites and activity level .This can be accomplished by putting forward original strategies for the preparation of perovskite and the hybrids containing them. Because of the interconnected nature of these factors, a change in the composition can directly affect the structure of crystal and vacancy of oxygen as well as the crystal structure. For example, in some circumstances, an increase can be observed in both the extrinsic and the intrinsic qualities simultaneously [35].

2.1 Composition of the Perovskite

By altering the catalyst's electronic structure, the inclusion of B-site over A-site components has a profound effect on the catalyst's activity. Combining the precious metal with the transition metal alters positive charge contribution of metallic ions on the A-site. As a result, not only is the oxidation state changed, but the orientation of cations containing transition metals is also likely to be changed, and an oxygen vacancies may be created[13]. Comparing the characteristics of doped precious metals at the A-site with transition metals at the B-site has comprised the majority of research. Starting with the findings for coating on the A-site and B-site dopant catalysts.

2.1.1 A-site Doping ($A_{1-x}A'_xBO_3$)

The most common application for lanthanum has been in the A-site position of the rare earth metal industry. Regardless of the stoichiometry and the route of synthesis,

A-site doping almost always results in an increase in the catalytic activity. Shao et al. [59] investigated strontium-based lanthanum La1-xSrxFeO$_{3-\&}$ (x=0-1) bases perovskite catalysts and identified with the higher activity of OER in alkaline media. Due to the oxidation of Fe^{2+} to Fe^{3+} and the compensation of charge that occurs when Sr^{2+} substitutes for La3+, a direct reduction in the lattice size occurs whenever there is an increase in the amount of Sr doping. Since Sr doping increases the activity, Jin et al. developed a unique LSM perovskite ($La_{0.8}Sr_{0.2}MnO_3$) having a high surface area of 48.2 m^2g^{-1}. This perovskite shows good efficiency for both ORR and OER reactions[60]. Tulloch et al. made a similar contribution by developing a $La_{1-x}Sr_xMnO_3$ perovskite by varying the values of X from 0 to 1 and finds that it is more active towards Oxygen reduction reaction (ORR)[61].

2.1.2 Doping of B-site ($AB_{1-x}B'xO_{3-\&}$)

Doping of B-site plays more effective role then the doping of A site because B-site provides more reactive site in typical processes suggested for OER/ORR. There are many transition metal oxides are present; the loading of these oxides at the B site influences the catalytic activity of perovskite based catalyst. Because of their high optimum energy, iron and nickel are the most abundant of these elements. The replacement of Fe at the B-site in $LaCoO_3$, that possesses the potential to boost the oxygen evolution reaction efficiency of oxides based on perovskite, was the subject of research conducted by Duan et al. [62]. The enhanced spin state of Co^{3+} in $LaCoO_3$, which was caused by the 10% substitution of Fe, led to good OER efficiency.

2.1.3 Doping of A/B site ($A_{1-x}A'_x B_{1-y}B'_yO_3$)

Morphology of material and generation of active sites are both increased by doping with rare earth metal as well as transition metal. In this particular situation, a more in-depth analysis is required in order to identify the ideal composition for elevated activity levels. The structural properties of the doped material can be transformed in different ways depending on the procedure that is used. There are a few distinct approaches that have been suggested for developing the quaternary perovskite catalyst, each of which would result in a different structure and set of catalytic capabilities. A perovskite doped with strontium was the subject of research conducted by Singh et al. [63], who investigated the effect that changing the metals in prepared catalyst in which B might be any of Cr, Fe, Cu, and Ni, had. The electro - catalytic characteristics of the above catalysts were investigated using CV, and it was determined that there was

a pair of redox peaks just prior to the beginning of OER. Because transition metals were substituted at the B-site, the surface roughness was massively enhanced, which resulted in a significant active surface area being provided.

Because of its excellent charge transferability, Perovskite oxides containing barium doped with strontium has been the subject of research for a significant amount of time. According to the findings of J. May et al. [64], $Ba_{0.5}Sr_{0.5}Co_{0.8}Fe_{0.2}O_{3-\&}$ (BSCF82) is the most effective electrocatalyst for the water oxidation reaction that occurs in an alkaline media. Through the use of HRTEM, the researchers investigated the durability of several different catalysts, such as BSCF82, $La_{0.4}Sr_{0.6}CoO_3$ (LSC46), $LaCoO_3$ (LCO), and $LaMnO_3$ (LMO), as well as modifications in surface morphology that occurred during OER. There is a negative correlation between the activity of OER and size of cobalt atoms. [64]. Jin et al.[60] Mentioned that their research on the electrochemical behaviour of $Ba_{0.5}Sr_{0.5}Co_{0.8}Fe_{0.2}O_3$ (BSCF) was conducted in the same region but with a distinct composition of rare earth metals (x=0.5). In alkaline environments, its effectiveness as a bi - functional electrocatalyst has been established beyond a reasonable doubt. The catalyst has a limiting current density that is equivalent to 20 weight percent platinum on carbon. However, the starting potential is less than Pt/C catalyst, when matched to the work performed by Jin et al. This is due to the BSCF perovskite catalyst exhibits diffusion limiting current density. This is because O_2 has different kinds of interactions with different kinds of electrocatalysts, and different kinds of species are adsorbed onto different kinds of transition metal cations. When used in an alkaline medium, BSCF demonstrates the potential to act as a bifunctional catalyst with useful applications [60]. To check the effect of precious metals like doping of in perovskite framework, Bu et al. [65] substituted Pr in a perovskite oxide congaing BSCF with large oxygen vacancies, which exhibits greater durability and excellent electrical conductivity. An especially significant rise in ORR and OER activity can be credited to the existence of greater oxygen vacancy levels and an oxidised state of cobalt. Within a potential ranging from 300mV-600m V, it demonstrated a high electron transfer number of between 3.77 and 3.89. Additionally, it demonstrated a stronger cycle stability and as a result, proved to create an encouraging future for oxygen reduction reactions.

Chang et al. [66] studied $La_{0.6}Ca_{0.4}Co_{0.8}Ru_{0.2}O_3$ powders generated by an unstructured citrate precursor technique for ORR. Their work resulted in the development of a very

durable replacement perovskite structure that is relied on ruthenium as the B-site dopant. A micro - porous structure resembling foam is produced, with pores ranging in size from 0.5 to 3.0 micrometres. Increased H_2O_2 deposited in the KOH media is responsible for this catalyst's enhanced catalytic efficiency. The outcomes of the polarisation curve experiments performed using $La_{0.6}Ca_{0.4}Co_{0.8}Ru_{0.2}O_3$, $La_{0.6}Ca_{0.4}Co_{0.8}Ru_{0.2}O_3$.

2.1.4 Doping of Main Group Element at Cation Site

An accepted pattern in studies had been the inclusion of transition metals and rare earth metals. However, a novel concept has been presented that involves doping of a compound having zero activity at the B-site. This concept could really help in the electronic framework adjustment of a metal which is active for reduction and, as a result, can increase the electrocatalytic efficiency. Shao et al. [67] studied using phosphorous, which is not a metal , doped on the positive ion site in order to build a novel perovskite oxide. This was done in to achieve their goal. The various phosphorous formulations, such as $La_{0.8}Sr_{0.2}Mn_{1-x}O_{3-\&}P_x$ (where x =0-0.1) were tested, and it was discovered that the phosphorous is dissolved at the 0.05 composition. The addition of 5% phosphorus not only boosts the electrocatalytic activity but also has a significant impact on the material's stability. This is because phosphorus has an exceptionally high electric conductivity and provides an excess of extremely reactive oxygen species. The LSMP0.05 demonstrated the maximum surface area of all of them for ORR which is calculated by BET [67], which was 27.3 $m^2\ g^{-1}$, and it also had the maximum kinematic current density, which was 2.97 mA cm^{-2}. This method has also been used on $SrCo_{0.95}P_{0.05}O_{3-\&}$ (SCP) [68] and Mo doping in $Ba_2CoMo_{0.5}Nb_{0.5}O_{6-\&}$ (BCMN) [69] compositions, and the findings represent that the material was extremely stable and had a high level of activity for OER. This method has allowed for the beginning of a new phase of study into the use of various perovskite oxides doped with non-metals as catalysts which are good for both OER and HER.

In order to obtain high activity, Shao et al. [70] created another strategy that was very similar to the first. Doping an iron-based perovskite with the earth-abundant Si metalloid SrFe0.9Si0.1O3 (SFSi) has been shown to increase the activity of oxygen evolution reaction (OER) of the perovskite. This freshly synthesised catalyst demonstrates an impressively low Tafel slope, indicating that it possesses an excellent

electrochemical characteristic. Doping electrocatalysts with elements that are rich in the earth leads to high-performance electrocatalysts that are also cost-effective[70].

2.1.5 Cation Deficient Perovskite

It is well-known that anion insufficiency is extremely popular, and a significant amount of research has been done in this field. However, cationic insufficiency is still a subject of investigation at this time. Because it makes it easier for hydrogen to adsorb, the non-stoichiometric structure of perovskites is advantageous for both OER and HERs. Zhu et al. [71] developed a catalyst with a cationic deficit on the A site which enhances the OER and ORR catalytic performance. The implementation of $LaFeO_3$ during an alkaline solution led to the discovery of definitive data for OER rather than ORR. Perovskites made from $La_{1-x}FeO_{3-\&}$ $L_{0.95}F$ demonstrated the highest efficiency for both reactions out of all the synthesized perovskites. The increased activity could be credited to the formation of oxygen vacancies at the surface as well as the existence of Fe^{4+} radicals inside A-site cation deficit perovskite. As a result of these findings, it has the capability to act as a bi-functional catalyst. Shao et al.[56] introduced a technique known as insitu exsolution to manufacture a catalyst having metal particles that were uniformly disseminated on the perovskite backbone. Exolved-$La_{0.4}Sr_{0.4}Ti_{0.9}Ni_{0.1}$ (LSTN), Ex-$La_{0.4}Sr_{0.4}Ti_{0.9}Co_{0.1}$ (LSTC), Ex-$La_{0.4}Sr_{0.4}Ti_{0.9}Fe_{0.1}$ (LSTF), Ex-$La_{0.4}Sr_{0.4}Ti_{0.9}Ni_{0.075}Fe_{0.025}$ (LSTNF), and Exolved-$La_{0.4}Sr_{0.4}Ti_{0.9}Ni_{0.05}Co_{0.05}$ (LSTNC) have all been created using the same method. In comparison to the others, Ex-LSTN exhibited the maximum activity for the HER. This was due to the existence of optimal free energy for H2 adsorption. However, Ex-LSTN exhibited the lowest catalytic activity for Oxygen Evolution Reaction, where C_o performed more effectively. Exolved $Sr_{0.95}Nb_{0.1}Co_{0.9-x}Ni_xO_{3-\&}$ (SNCN) was recently developed by Islam et al. [72] wherein Nickel cobalt nanoparticles had experienced the process of exolving. Liu et al. [73] also generated cation deficit $Sr_{1-x}Nb_{0.1}Co_{0.7}Fe_{0.2}O_{3-\&}$ (x = 0.02, 0.05, and 0.1), indicated as S0.98NCF, S0.95NCF, and S0.90NCF. This resulting in shrinkage in the crystal structure as well as different oxidation states.

2.2 Perovskites with Oxygen Deficiencies

When oxides with oxygen deficiencies are created, the outcome is an instant filling and generation of interlayer oxygen vacancies. These interlayer oxygen vacancies plays critical role in the OER/ORR and HER activities that are essential to the oxides. Because of the high correlation between catalytic activity and oxygen shortage

concentration, the resultant structure is deformed and does not have a cubical shape. As per the results of Mefford et al. [57], the OER performance of the $La_{1-x}SrxCoO_{3-\&}$ series depends on the concentration of oxygen vacancy, where the maximum activity being achieved on $SrCoO_{2.7}$, which also had the maximum number of vacancies. Yuasa et al. [74] presented their research on LSFM prepared using the reverse miscella method with (x = 0-0.4) and (y = 0-0.8) in order to develop the distinctive features for ORR. The ORR activity of the $La_{0.6}Sr_{0.4}Mn_{0.8}Fe_{0.2}O^{3+}$ charged electrode was discovered to be greater than Pt/C electrode at current densities more than 80 mA cm^{-2}; however, this activity was shown to decrease when the current density was decreased. Despite the fact that the performance improved with increasing x and deteriorated with rising y, the oxides generation for bigger x was not adequate. perovskite oxide having the value of X and Y is 0.2 was used for the stability test, the results were substantially more reliable [74].

The researchers Singh et al. [75] studied on a sort of perovskite that had the formula $MMoO_4$, where M might be either cobalt, iron, or nickel. When Cr_2 $(MoO_4)_3$ doped with Cr it helps to decrease the Tafel slope value which cause the increase in catalytic activity. When oxygen deficiencies are introduced into a material, a variety of different kinds of structures are produced. According to Zhou et al. [76] the crystal structure has a significant impact on the catalytic activities. The studies were carried out on various crystalline forms of $LaNiO_3$ that were produced by heating the material at temperatures of 400 ^oC, 600 ^oC, and 800 ^oC respectively. When the structure changed from rhombohedral to cubic, there was an accompanying improvement in the ORR/OER performances. Longer Ni-O bonds in a cubic configuration are conducive to excellent OER/ORR performance[76].

Cheng et al.[77] examined the oxidation number of manganese in perovskite oxides as they progressed through their work with oxygen-deficient perovskite. It has been suggested that the electrocatalytic performance of non-stoichiometric $CaMnO_{3-\&}$ type perovskite can be improved by employing a suitable approach, which will result in the formation of oxygen deficiencies. This method would involve the introduction of the facile approach. The research was continued by Kim et al. [78], who announced the $Ca_2Mn_2O_5$ electrocatalyst for OER in alkaline media. They discovered that the electrocatalyst was catalytically more active than the $CaMnO_3$ that Zhang et al. [77] had reported. $Ca_2Mn_2O_5$ exhibited a mass activity for OER at 30.1 A/g at 1.70 V

relative to RHE. The porous structure and electronic configuration of manganese are among the most potential factors for the improved activity. The reductive annealing procedure, which was used to create the catalyst in a novel manner, proved to be the factor that made the difference. This catalyst's crystalline form allows for the better transit of OH- ion, which is one of the factors that contributes to the catalyst's high activity.

The capabilities of oxygen-deficient perovskite could be improved further by using an appropriate approach to create comparatively tiny nanomaterials as an electrocatalyst. This will allow for the perovskite to be more effective. The barium-based oxygen-deficient bifunctional electrocatalyst was discussed in Chen et al. [79]'s research. It has been reported that $BaTiO_{3-x}$ nanoparticles may be generated using the sol-gel method. These nanoparticles demonstrate an OER activity that is significantly greater than that of expensive noble metals synthesized using a process that is very comparable. It has shown substantially that in comparison to IrO_2, and it has greater oxygen vacancies, both of which are accountable for simpler adsorption and the electron transport phenomenon observed in OER.

As is common knowledge, when the transition metals are introduced in the cathode site the electrocatalytic activity is increased due to the generation of oxygen vacancies. Wang et al. [80] claimed that they had successfully doped nickel to a perovskite containing manganite and likened it to a catalyst which was not doped. For their ORR and OER activities, both were made using a simple sol-gel method for the preparation. The presence of a considerable amount of Ni^{3+} on the surface, which was brought about by the addition of Ni, resulted in an increase in the number of oxygen vacancies, which in turn resulted in an increase in the catalytic activity. The produced catalyst demonstrated that it has substantially decreased overpotential and very stable showing 79 cycles inside a voltage range of 2.0 to 4.8 V (compared to Li^+/Li), which can be compared to Pt/C but comes at a far more affordable price. Doping can also be accomplished successfully with metals from the P block since these metals have excellent conducting characteristics. $Ca_xLa_{1-x}Al_{1-x}Mn_xO_{3-\&}$ perovskite oxides were successfully synthesised by Christ et al. [81]. The researchers' ultimate goal was to design an electrocatalyst which shows excellent electrocatalytic activity towards oxygen reduction reaction. $Ca_{0.9}La_{0.1}Al_{0.1}Mn_{0.9}O_{3-\&}$ (9119) was discovered to have the most homogeneous elemental dispersion of any of the samples that were prepared

using the SS process. In terms of its electrochemical characteristics, it also demonstrated the best level of performance. The prepared electrocatalyst shows the surface area of 6.1 m^2g^{-1} and mass activity of 108 mA mg^{-1}. The same sample was tested for various techniques; however, aerogel method managed to produce the highest surface area. Jing Xia et al.[82] took a new approach by adding P block elements to A site which results in the generation of more active sites due to the non-stoichiometric behaviour of oxygen. P block elements have the dual nature because of the unfilled d orbitals. This dual nature helps the charges to follow effectively on the active sites present on the surface of material. Another type of perovskite was made by Shao et al. [83] using a different method having low overpotential and good surface area which results in good electrocatalytic activity towards OER.

A wide-ranging area of research that, in conjunction with oxygen shortage, is predicated on the creation of a layered structure that improves water dissociation characteristics, hence making hydrogen adsorption easier. Sr_2RuO_4 oxide was the layered metal oxide that was created by Shao and colleagues [84] for use in the hydrogen evolution reaction. Along with a high current density of 0.898 mA cm^{-2}, the electrocatalyst demonstrated very low Tafel slope and overpotential, both of which were very low. This electrocatalytic activity of prepared catalyst is due to the presence of SrO which helps to flow the charges to the active sites.

The structure of a catalyst is a significant factor in determining its properties. The catalyst is always improved by the addition of nanostructured materials, which have excellent catalytic capabilities. A Nano rod of oxygen-deficient perovskite-type oxide was prepared thanks to the efforts of Shao and colleagues [85]. For the synthesis of $SrNb_{0.1}Co_{0.7}Fe_{0.2}O_{3-\&}$ perovskite nanorods, the simple electrospinning approach was adopted. As a result, this catalyst shows outstanding electrochemical properties. Due to the unique structure of the catalyst, SNCF-NR showed an overpotential value of 390 mv at current density of 10 mA cm^{-2}. After the calcination process, the catalyst shatters into a structure resembling nanorods that have an average diameter of 100 nanometres. With an output of an extremely high current density, it is suitable for both open- and closed-loop energy recovery applications. Deganello et al. [86] took a different approach when they worked on the preparation of $La_{0.6}$ $Sr_{0.4}Fe_{0.6}Mn_{0.4}O_{3-\&}$ (LSFM). As a result of their efforts, they produced a highly active catalyst with a high surface area that showed better result for ORR and OER. The inclusion of silicate led

to an increase in the onset potential for ORR, and the authors propose keeping the percentage of Si in the material at or below 4 weight percent. Despite this, oxygen deprivation in conjunction with cation site the electronic configuration of material also effects the electrocatalytic activity as suggested by Zhou and Shao[31]. In this work he tends to enhance the electrocatalytic activity of prepared catalyst by tuning the crystal lattices. Iron dopants enhances the catalyst's potential to accelerate a reaction. In coupled with massive doping, the construction of a three-dimensional high porous structure in $LaFeO_3$ (LF) is key for the material's high catalytic efficiency as well as its stability. The results that were obtained for 20% cobalt doping during the HER have genuinely produced a stable electrocatalyst which has more active sites.

2.2.1 Cation Ordered Double Perovskite

The unique layer structure provides remarkable electrocatalytic activity and stability towards the perovskites. Most recently, Shao et al.[87] conducted research in a field that is quite comparable to this one. In this research they summarized that the generation of more active sites helps to increase the electrocatalytic activity and this provides a channel to flow the ions quick because of the different reaction paths. The primary objective of the research was to develop a double perovskite of the formula $Sr_2Fe_{0.8}Co_{0.2}Mo_{0.65}Ni_{0.35}O_{6-\&}$ that possessed several active sites in order to improve the OER activity of the electrocatalyst. As a highly effective OER and ORR catalyst, Sun et al. [69] developed a perovskite having which is highly active for both OER and ORR. The perovskite had a compositional formula of $Ba_2CoMo_{0.5}Nb_{0.5}O_6$ (BCMN) and $Ba_2Co_{1.5}Mo_{0.25}Nb_{0.25}O_{6-\&}$ (BC1.5 MN). The latter has demonstrated a lower overpotential of 40 $mVcm^{-2}$ and a mass activity that is 3.5 times higher than that of BCMN. The sol-gel approach was used to produce another B-site doped perovskite called $Ba_2Bi_{0.1}Sc_{0.2}Co_{1.7}O_{6-\&}$ (BBSC), which shows excellent stability in comparison with other catalysts. When catalysts measured at a potential of 0.5V, the specific activity of disorderly ordered $Ba_{0.5}Sr_{0.5}Co_{0.8}Fe_{0.2}O_{3-\&}$ (BSCF) and $Ba_2Bi_{0.1}Sc_{0.2}Co_{1.7}O_{6-\&}$ (BBSC) was found to be lower. The B-site ordering was shown to have had a substantial impact in the enhancement of OER activity. To put it simply, the increased activity is due to the effective charge transfer[88].

Perovskite composites with decreased graphene oxide have shown very high catalytic results, which could be improved upon by inducing oxygen vacancy. This was mentioned earlier. Significant research on perovskite oxides was reported by Kim et

al. [89], who created triple perovskites and demonstrated that $Nd_{1.5}Ba_{1.5}CoFeMnO_{9-\&}$ shows excellent electrocatalytic activity towards ORR and OER. The electrocatalytic activity was enhanced due to the unique morphology of prepared catalyst. Which helps in the formation of active sites and movement of charges.A nonstoichiometric ratio of oxygen to electronic configuration is the primary cause of NBCFM's increased catalytic activity. This is due to NBCFM's unique electronic configuration. Due to the fact that the triple perovskite-type oxide generates massive oxygen vacancies [89], which were produced as a result of the structural distortion that was brought about by continuous stacking. Wang et al. [90] investigated the human oestrogen receptor (HER) activity of a number of H_2 reduction treated $NdBaMn_2O_6$ double perovskites with varying amounts of oxygen vacancy (= 0.35, 0.54, and 0.80). The value of = 0.54, which was deemed to be the result of a variety of characteristics, including deformed structure, near-unity eg occupancy, and O-p band centre, displayed the highest level of activity. This value was regarded to be the best. As a result, the development of oxygen-deficient perovskites should proceed with caution.

2.3 Nanostructured Perovskites

Large in size but with a modest surface area, the bulk perovskites possess limited catalytic properties. The development of the catalyst on the nano-scale not only results in the production of a compound that is diversely active and has a great phase purity, but it also increases the structural features of the catalyst, which results in the production of additional active sites. Perovskite containing La at the A-site has been the subject of extensive study. Simply altering the transition earth metal present in the B-site can lead to the production of a wide variety of distinct catalytic characteristics. Hardin et al. [91] developed $LaNiO_3$ nanocrystals that displayed exceptional electrocatalytic activity towards oxidation and reduction reactions due to high porosity, high surface area, and incorporation of a OH into a lattice structure. Taking Co as the B-site element and generating an amorphous surface through a hydrothermal procedure, as developed by Kim et al. [92], improved the structural properties of perovskite. This study focuses on the development of nanoporous structures and spheroids of $LaCoO_3$. The shape and electrochemical characteristics of a perovskite-type oxide were assessed. A rhombohedral unit cell structure was discovered, and it had truncation at specified corners. This can be explained by the fact that the stoichiometric ratio of the metal precursors to the organic molecules was not consistent

2.4 Perovskite on Material Support

The catalytic effectiveness can be significantly influenced by promoting the catalyst on a particular material. This could be achieved by generating more active site which helps in the movement of ions effectively which results in high electro catalytic activity. The generation of more active sites could be achieved by controlling the morphology of catalyst. Perovskite could be supported on a wide variety of materials, based on the specific property that is being searched.

Tiwari et al. [93] prepared a catalyst by coating perovskite on conductive material. They synthesised electrocatalyst $La_{1-x}Sr_xCoO_3$ (x = 0, 0.2, and 0.4) using two different methods. This showed excellent electrocatalytic activity toward HER having the overpotential value of 175 mV, 130 mV and 75 mV for $LaCoO_3$, $La_{0.8}Sr_{0.2}CoO_3$, and $La_{0.6}Sr_{0.4}CoO_3$ respectively at 10 mA cm^{-2}.

Carbon can directly influence the electrocatalytic activity of catalyst. Tachibana et al. [94] supported the LCMF perovskite on the carbon and they use miscella approach for the preparation of this catalyst. For the preparation of this carbon-supported catalyst, the reverse miscella approach using $KmnO_4$ was selected as the method of choice due to its high Mn valency. It was discovered that doping Ca increased oxygen reduction capacity, which can be compared to Pt/C. Hsieh et al. [95] used CNCs as supporting material for Ir coated $La_{0.6}Ca_{0.4}CoO_3$ perovskites, which resulted in carbon being a better support material for perovskite. A further conclusion that can be drawn is that the perovskite that was produced by the solid-state reaction has an asymmetrical form and ranges in size from 100 to 250 nanometres. The $La_{0.6}Ca_{0.4}Co_{0.8}Ir_{0.2}O_3$/CNCs catalysed GDE had excellent catalytic performance by having high current density value. This electrocatalyst has shown bifunctional electrocatalytic activity which is better than $La_{0.6}Ca0.4CoO_3$ catalyst. Another sort of nourishment that is beneficial to the rapid reduction of oxygen can be of an oxophilic nature, which results in an increase in the amount of oxygen that is absorbed. According to Park et al. [96], the use of Ag greatly improves the water activation on LMO, which in turn boosts the ORR activity. It has been established that the order ($Ag/LaCoO_3$ $Ag/LaFeO_3$ $Ag/LaMnO_3$) applies to the electrocatalytic activity, which depend on oxophilic nature. This is because the catalytic activity supports the activation of water, which in turn promotes the ORR. The transfer of charge from manganese to silver, as well as an increase in the oxophilic character of manganese sites, both contribute to an

improvement in the adsorption of oxygen species. As a result, it is recommended that the support that is utilised have a highly oxophilic character in order to lessen the amount of interference that occurs between the catalyst and the support [96].

2.5 Perovskite Composites

Designing a hybrid of perovskite with another material of comparable significance offers a novel approach to the problem of getting high catalytic activities in a material. Using nanoparticles of noble metals in the development of the composite can increase the current density while simultaneously reducing the overpotential. Soares et al. [124] introduced a novel concept for the fabrication of composites made of PtRu/C-$LaNiO_3$[97]. The catalytic performance of the composite material on the nickel foam support has seen a significant boost as a result of the inclusion of Pt-Ru nanoparticles. The elemental dispersion map revealed that the nanoparticles got dispersed evenly across the electrode's surface. The oxygen that is created during the anodic sweep causes a reduction, which in turn produces a cathodic spike at an energy level of -200 mV. Following the observation of the clearly defined redox peaks was an increase in value of current that occurred at a potential that was more than 0.6V. After operating for 50 cycles, variations in voltammetric curves were recorded, which suggested an elevation in catalytic activity in OER. This result can be caused by a rise in surface roughness. Because of this, the mobility of the electrolyte to the active site is improved.

Han et al. [98] presented an alternative method for manufacturing a hybrid with Pt. They prepared clusters of platinum which was supported on perovskite like $CaMnO_3$. This was a unique technique for the preparation of a hybrid with Pt. Two-dimensional materials, in addition to precious metals, have been suggested for use as an active catalyst. Chong et al. [99] synthesised the hybrid materials ($LaNiO_3$-N-S-Gr.) to minimize the resistance offered by charge transfer and to gain good stability. G Kim [100] published his research on 3D porous nitrogen-doped graphene with a $(PrBa_{0.5}Sr_{0.5})_{0.95}Co_{1.5}Fe_{0.5}O_{5+\&}$ (PBSCF) perovskite, which he referred to as P-3G. The overall findings were extremely encouraging, particularly with regarding to oxidation and reduction reactions. By analysing it can be summarised that enhancement of electrocatalytic activity towards hydrogen production is because of the movement of ions on the active sites. And due to effective movement of ions this hybrid electrocatalyst shows excellent activity by having low Tafel slope values and high

current densities. Advancements in the perovskite for oxidation and reduction reactions can be seen in **Fig. 6**.

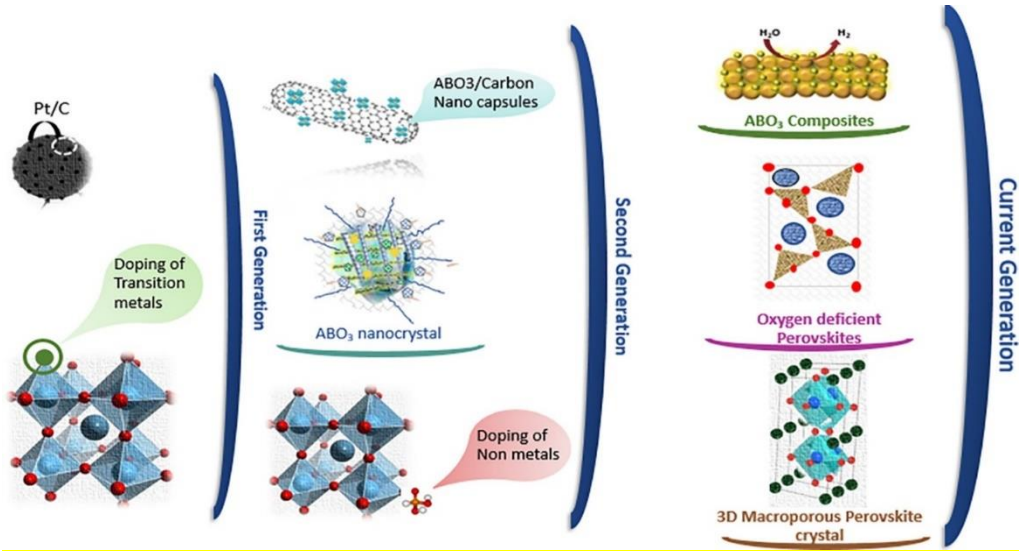

Figure 6 *Advancements in the perovskite for oxidation and reduction reactions*

The physicochemical features of perovskite electronic configuration can be taken into account in order to calculate the intrinsic increase in activity that occurs at each reactive site. These characteristics include a broad diversity of composition, which was accomplished through several processes like as substitution, oxygen vacancies, and the formation of a variety of crystal forms[72]. The alternative method is to extrinsically boost both the activity level and the total number of active sites on the surface, which is a function of the geometric impact. This can be accomplished by putting forward original strategies for the production of perovskite nanoparticles and the composites containing them. Because of the interconnected nature of these factors, a variation in the composition may directly influence the oxygen vacancies along with the crystal structure.

In this work, it has been tried to develop bifunctional electrocatalyst, which is cost effective as well as highly stable. Hybrids of LSTN/g-CN have been prepared by insitu sol gel method to increase their activity and make them comparable to state-of-the-art catalyst. The extensive literature review has been done on various type perovskite oxides as well as their composite. LSTN perovskite and graphitic carbon nitride hybrid material is prepared and characterised to explore the importance in practical application for hydrogen production.

Chapter No 3

Materials and methods

3.1 Materials

Materials used in the preparation of LSTN/g-CN consists of lanthanum nitrate hexahydrate ($La(NO_3)_2.6H_2O$), strontium nitrate ($Sr(NO_3)_2$, titanium n-butoxide ($C_{16}H_{36}O_4Ti$), Nickel (II) nitrate hexahydrate ($Ni(NO_3)_2.6H_2O$), Citric acid ($C_6H_8O_7$), EDTA-2Na dihydrate ($C_{10}H_{14}O_8N_2Na_2.2H_20$), ethanol (97wt%). All of these materials were procured from Sigma Aldrich USA.

3.2 Synthesis of LSTN Perovskite

For the synthesis of $La_{0.4}Sr_{0.4}Ti_{0.9}Ni_{0.1}O_{3-\&}$ sol gel method was used which was followed by calcination at high temperature. In 100 ml DI water, 16m moles of $La(NO_3)_2.6H_2O$, 16m moles of $Sr(NO_3)_2$, and 4.5m moles of $Ni(NO_3)_2.6H_2O$ were dissolved for the preparation of catalyst. In above solution, 4.5m moles of $C_{16}H_{36}O_4Ti$ was added drop by drop at 80°C under constant stirring. The complexing agents EDTA-2Na dihydrate ($C_{10}H_{14}O_8N_2Na_2.2H_2O$) and anhydrous Citric acid ($C_6H_8O_7$) were then added with continuous stirring in a molar ratio of 1:2. To stabilize the solution's pH, 1 M of strong basic NH_3 was added. The solution was then heated to 150 degrees Celsius on a hot plate until a transparent gel formed. The gel was then heated at 300°C for 9 hours and the solid powder was achieved. To remove organic compounds solid powder was calcined at 1000°C for 10 hours and then the desired product formed. As shown in **Fig. 7**;

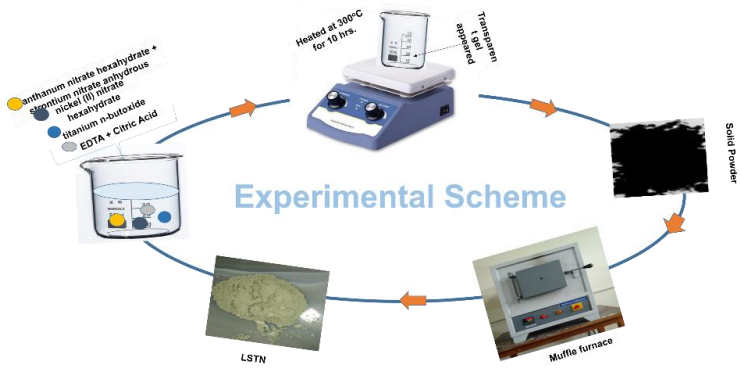

Figure 7: *Synthesis of LSTN perovskite*

3.3 Synthesis of g-C_3N_4

In crucible 5.0 gram was placed then this crucible was placed in muffle furnace at 550^{o}C for 3 hours at the heating rate of 2^{o}C min^{-1}. After heating solid powder was formed having light yellow colour and then it was sonicated for 1 hour in probe sonicator to break its sheets. Then ultra-centrifugation step was done to obtain the solid powder and then it was placed in vacuum oven at 60^{o}C for 12 hours to remove moisture content and finally light yellow colour powder named g-C_3N_4 is formed. As shown in **Fig. 8**;

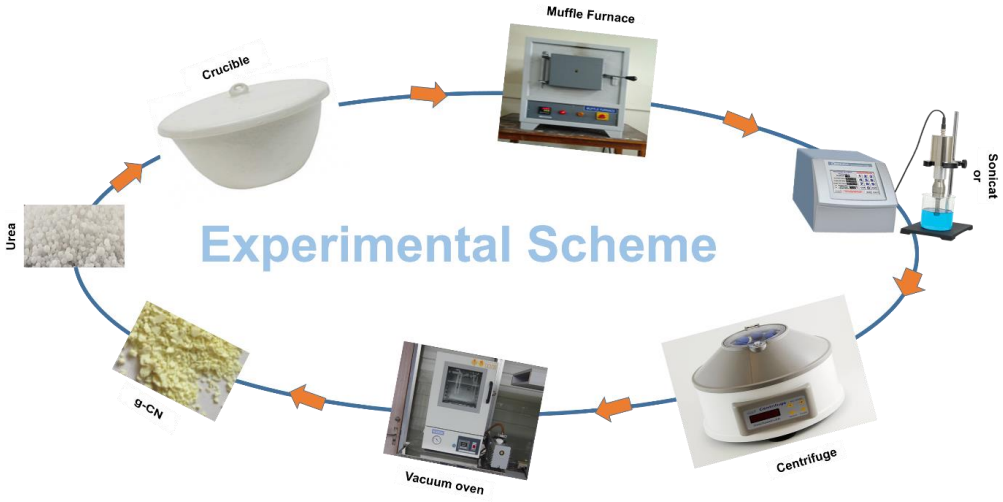

Figure 8: *Synthesis of g-C_3N_4*

3.4 Synthesis of LSTN/g-C_3N_4 Hybrid

In crucible 5.0 gram was placed then this crucible was placed in muffle furnace at 550^{o}C for 3 hours at the heating rate of 2^{o}C min^{-1}. After heating solid powder was formed having light yellow colour and then it was sonicated for 1 hour in probe sonicator to break its sheets. Then ultra-centrifugation step was done to obtain the solid powder and then it was placed in vacuum oven at 60^{o}C for 12 hours to remove moisture content and finally light yellow colour powder named g-C_3N_4 is formed. And then for the synthesis of LSTN/g-CN hybrid, sol gel method was used which was followed by calcination at high temperature. In 100 ml DI water, 16m moles of $La(NO_3)_2.6H_2O$, 16m moles of $Sr(NO_3)_2$, 4.5m moles of $Ni(NO_3)_2.6H_2O$ and 1 wt.%, 3wt.%, 5wt.%, 8wt.% of g-CN respectively were dissolved for the preparation of catalyst. In above solution, 4.5m moles of $C_{16}H_{36}O_4Ti$ was added drop by drop at 80^{o}C under constant

stirring. The complexing agents EDTA-2Na dihydrate ($C_{10}H_{14}O_8N_2Na_2.2H_2O$) and anhydrous Citric acid ($C_6H_8O_7$) were then added with continuous stirring in a molar ratio of 1:2. To stabilize the solution's pH, 1 M of strong basic NH_3 was added. The solution was then heated to 150 degrees Celsius on a hot plate until a transparent gel formed. The gel was then heated at 300°C for 9 hours and the solid powder was achieved. To remove organic compounds solid powder was calcined at 1000°C for 10 hours and then the desired product formed. As shown in **Fig. 9**;

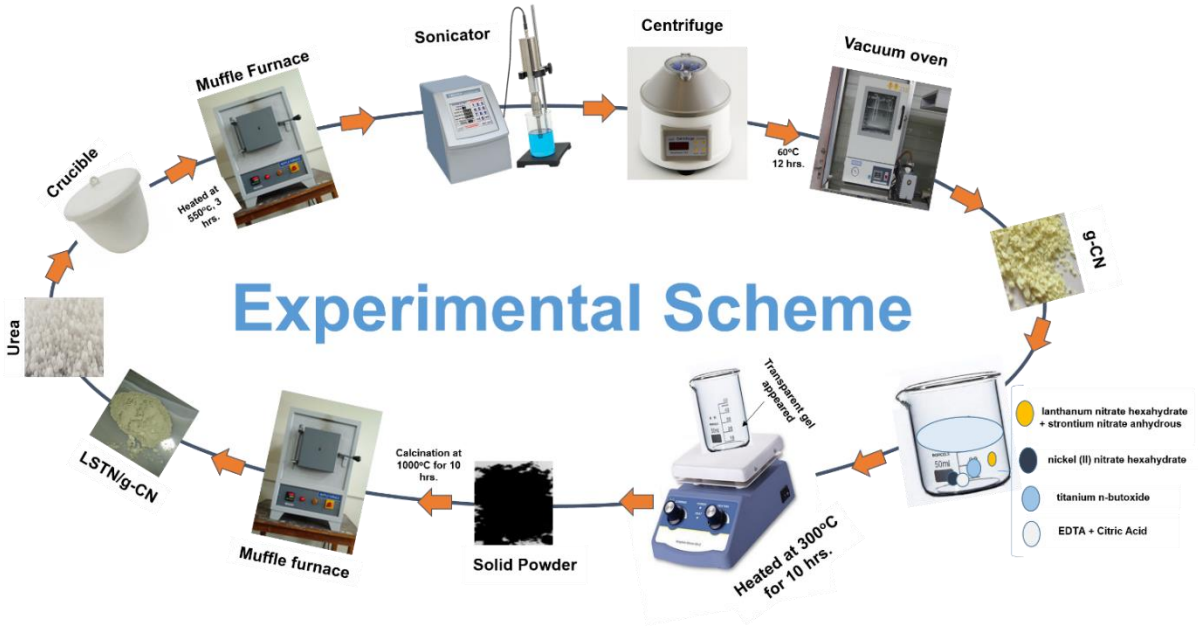

Figure 9: *Experimental Scheme for LSTN/g- C_3N_4*

3.5 Synthesis of LSTN Electrode

Ni is used as substrate to prepare the LSTN electrode. Preparation of LSTN electrode consist of three steps, in first step Ni foam was treated. For the treatment of Ni foam, it sonicated with 1 M HCL solution followed by Ethanol and DIW, for 30 minutes each. After sonication Ni foam was dried in vacuum oven for 3 hrs at 70°C. In second step Ink was prepared by adding 4-5 mg LSTN catalyst in 80µl Ethanol and 20µl Nafion as binder then sonicate it for 6 hours. In third step Ink was deposited on treated NF and followed by overnight drying at 80°C in vacuum oven. And by that LSTN electrode is prepared.

3.6 Synthesis of g-C_3N_4 Electrode

NF is used as substrate to prepare the g- C_3N_4 electrode. Preparation of g- C_3N_4 electrode consist of three steps, in first step Ni foam was treated. For the treatment of Ni foam, it sonicated with 1 M HCL solution followed by Ethanol and DIW, for 30 minutes each. After sonication Ni foam was dried in vacuum oven for 3 hrs at 70^{o}C. In second step Ink was prepared by adding 4-5 mg g-C_3N_4 catalyst in 80µl Ethanol and 20µl Nafion as binder then sonicate it for 6 hours. In third step Ink was deposited on treated Ni foam and followed by overnight drying at 80^{o}C in vacuum oven. And by that LSTN electrode is prepared.

3.7 Synthesis of Bifunctional LSTN/g- C_3N_4 Hybrid Electrode;

NF is used as substrate to prepare the g-C_3N_4 electrode. Preparation of LSTN/g-C_3N_4 electrode consist of three steps, in first step Ni foam was treated. For the treatment of Ni foam, it sonicated with 1 M HCL solution followed by absolute Ethanol and DIW, for 30 minutes each. After sonication Ni foam was dried in vacuum oven for 3 hrs at 70^{o}C. In second step Ink was prepared by adding 4-5 mg LSTN/g-CN catalyst in 80µl Ethanol and 20µl Nafion as binder then sonicate it for 6 hours. In third step Ink was deposited on treated Ni foam and followed by overnight drying at 80^{o}C in vacuum oven. And by that LSTN/g-C_3N_4 hybrid electrode was prepared.

3.8 Characterization Techniques

3.8.1 X-ray Diffraction (XRD)

Crystalline nature of LSTN, g-CN, LSTN/g-CN hybrids, was determined by using the X-RAY diffraction technique. A current of 40 mA and a voltage of 40 kV were applied. With a step time of 0.5 seconds per step, the sample was scanned at a step size of 0.04. The range of the scan angle 2θ was (10° to 80°). CuK radiation had a wavelength of 1.540A^o. X-ray diffraction is used to analyze the atomic spacing and crystal structure.

3.8.1.1 Objectives of XRD

The objectives of XRD is to identify of crystallinity of material. It is used to distinguish between crystalline and amorphous forms. It is also used to calculate lattice spacing of material. And also to find the average particle size.

3.8.1.2 Working Principle

Constructive interference among monochromatic X-rays is the basis for the XRD's working. Cathode ray tubes are responsible for the generation of X-rays, which are then subjected to filtering in order to produce monochromatic radiations. Collimation is the process of concentrating light rays in order to direct them toward the specimen. Constructive interference is produced as a result of the interaction among these rays and the specimen, which proves that Bragg's Law is valid. According to Bragg's Law, there is a one-to-one correlation between the lattice spacing and the diffraction angle of the specimen and the wavelength of the electromagnetic radiations. The representation of brag's law is shown in **Fig. 10** .It is also possible to write it as$n\lambda = 2d\ sin\theta$

Where;

n=integer λ= wavelength

d= interlayer spacing sinθ= Diffraction angle

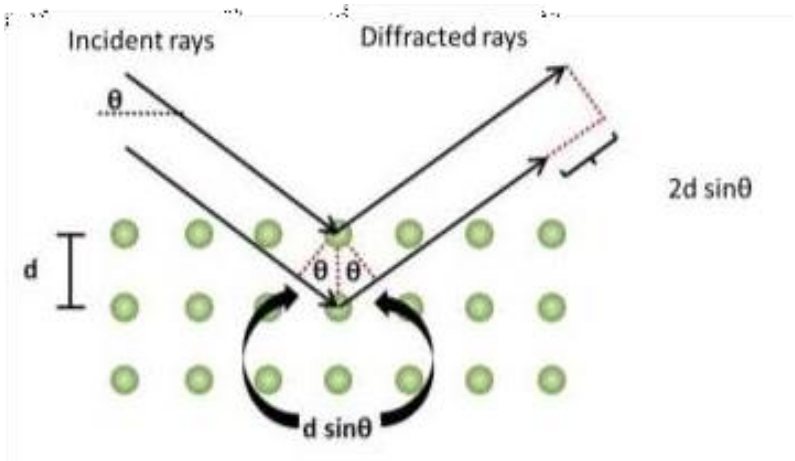

Figure 10: *Schematic's of Bragg's law[88]*

3.8.2 Fourier Transform Infrared Spectroscopy (FTIR)

In order to investigate the interfacial interactions between two phases involving the development of a hybrid, FTIR was used. In order to conduct the analysis, the Fourier Transform Infrared Spectroscopy (ATR-FTIR, BRUKER) machine was used. The analysis was performed in the frequency range of 4000-500 cm-1, with a resolution of 4 cm-1, and a scanning frequency of 32 was used.

3.8.2.1 Objectives of FTIR

The objective of FITR is to recognize organic, polymeric or sometimes inorganic compounds, characterization of unknown materials, and identification of contaminations (in or on the materials). In failure analysis, identify decomposition, oxidation or uncured substances.

3.8.2.2 Working Principle;

The FTIR works on absorbance of light by molecules, while they are in infrared region of the electromagnetic region. The absorption of light uniquely implies to the bonds which exists inside molecules. The infrared spectrum ranges from 12,800 to 10 cm-1 and is subdivided into near, middle, and far infrared[101].

Table 1: *Infrared Ranges in FTIR*

Sr. No.	Infrared Region	Frequency Range cm^{-1}
1	FAR IR	4000-12800
2	MID IR	20-4000
3	NEAR IR	50-1000

Infrared absorption spectrum mechanism is based on vibrations of molecules. When the specimen is exposed to radiations, its molecules absorb radiations of certain wavelength. This changes the dipole movement of specimen molecules. As a result, the energy level of the specimen molecule is transfer to excited state from the ground state. The energy gap determines the frequency of absorption peak. The change in intensity is subjected to the dipole moments and shift of energy levels.

3.8.2.3 Components of FTIR

The basic components of FTIR are source, Interferometer, Sample compartment, Detector, Amplifier, A/D Converter, Computer. The radiations are generated by the source. These radiations after passing through the interferometer reaches the specimen and are recognized by the detector. The signals are amplified by means of amplifier, are converted to digital signals by analog-to-digital converters. The signal is then transmitted to a computer wherein Fourier Transformation is performed. As shown in **Fig. 11** [90];

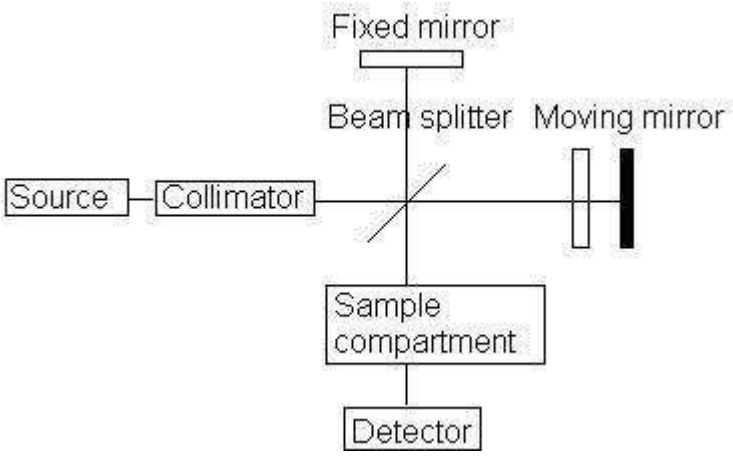

Figure 11: *Components of FTIR*

3.8.3 Raman Spectroscopy

Light is used in this molecular spectroscopy technique, which causes it to interact with the specimen in order to obtain information about its characteristics. To gain an understanding of the spectrum that is distinctive of particular vibrations of a molecule, it scatters light rather than absorbing light like FTIR does, and this is how it works. In addition to this, it offers details regarding shorter wavelengths modes & vibrations that are extremely helpful for gaining a fundamental comprehension of both the crystal lattice and the basis of the molecular structure. Principle of Raman spectroscopy is represented in **Fig. 12**.

3.8.3.1 Working Principle

The light's interaction with the molecules available in gas, liquid or, solid, the photons within incoming light get dispersed with same energy as that of incident photons, thereby undergoing elastic scattering. Only a small number among them undergo inelastic scattering. Raman helps user to capture vibrational characteristic signature of

molecule that develops an understanding of how they are put together as well as their method of interaction with other molecules around it[88].

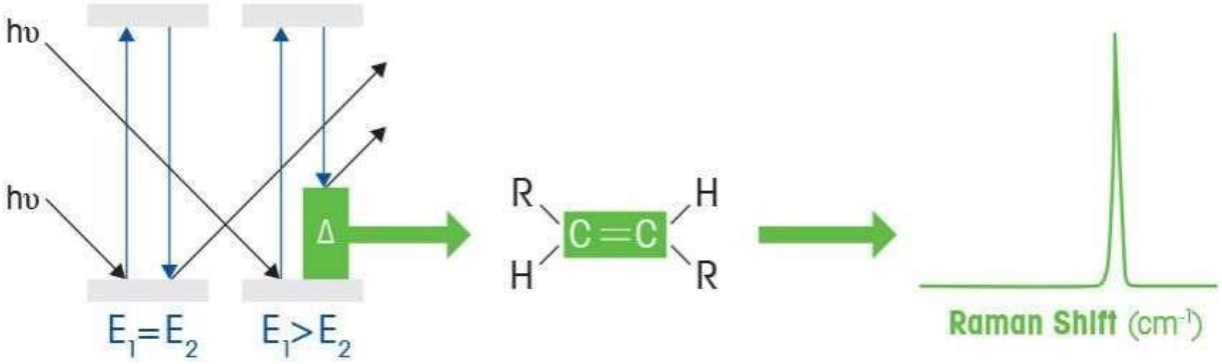

Figure 12: *Schematic illustration Raman spectroscopy principle*

3.8.4 Scanning Electron Microscopy (SEM);

The morphology of perovskites and its hybrids were recognized by SEM (JSM-64900). Prior to analysis, powder of material was placed on stud and gold plated to provide a conductive layer.

3.8.4.1 Objective of SEM

SEM is an outstanding technique for observing the surface of material and provides excruciate details about surface projections. It provides information about Texture (External Morphology), Chemical composition, Orientation and Crystalline Structure.

3.8.4.2 Working Principle

. When electrons are accelerated through a scanning electron microscope (SEM), they carry substantial quantities of kinetic energy with them. This energy is released as a wide range of signals created through electron encounters whenever the incident electrons are slowed significantly in the solid sample. These signals consist of secondary electrons (which are responsible for the production of SEM images), backscattered electrons (BSE), diffracted backscattered electrons (EBSD), photons (characteristic X-rays that are utilised for elemental analysis and continuum X-rays), visible light (cathode luminescence CL), and heat. Imaging samples typically involves the employment of secondary electrons and backscattered electrons. Secondary electrons are most useful for illustrating morphology and topography on samples, whilst backscattered electrons are most useful for illustrating disparities in substance in multiphase samples (i.e. for rapid phase discrimination). The creation of X-rays is

caused by inelastic collisions between incident electrons and electrons in discrete orbitals (shells) of atoms in the sample. This results in the release of X-rays. When excited electrons fall back to lower energy states, they produce X-rays that have a consistent wavelength therefore, distinctive X-rays are generated for every element in a material that is "stimulated" by an electron beam. This occurs when the electron beam passes through the mineral. Because the x-rays produced via electron interactions don't really cause a loss of quantity in the sample, scanning electron microscopy analysis is referred to as "non-destructive." As a result, it is able to perform SEM analysis for the same materials more than once.

3.8.4.3 Components of SEM

The components of SEM include electron source, condenser lens, scan coils, objective lens and secondary electron detector. Electrons are produced by the electron source, which is located at the very top of the column. This results in the production of an electron beam. Emission of electrons occurs when the electrons' thermal energy is greater than the work function of the source. These electrons then become accelerated, and the anode draws them to itself. The diameter of electron beam is adjusted by means of lens. If it is weakened, a broader beam is produced and vice versa. The path of electrons is also controlled by the lens. Electromagnetic lens is utilized owing to the fact that electrons couldn’t pass through the glass. Firstly, the electrons meet the condenser lens. After converging by condenser lens, the electrons are further condensed by the objective lens[102]. Components of SEM is shown in **Fig. 13**.

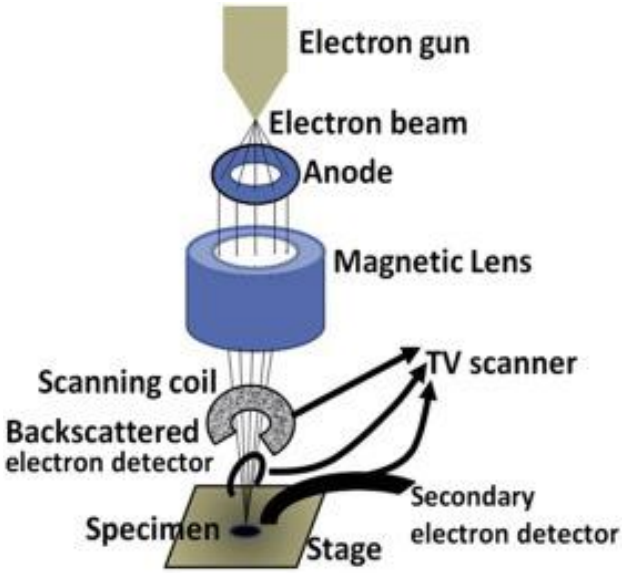

Figure 13: *Components of SEM*

3.8.5 Transmission Electron Microscopy (TEM)

The Transmission electron microscope uses an electron gun that utilizes electron beam to display he image of specimen. It is having high magnification power approx. 2 million times as compared to light microscope.

3.8.5.1 Working Principle

The working principle is similar to light microscope, except it uses a beam of electron to focus rather than light. As electron exhibit shorter wave length and thus an increase in resolution power occur when electron illuminates, which increases the electron transmission. It has three major working units.

1. Electron gun.

2. Image producing unit.

3. Image recording unit.

3.8.6 Energy dispersive X-ray spectroscopy (EDS);

The technique known as energy dispersive x-ray spectroscopy is currently one of the most common methods for determining the elemental composition of a material. It majorly works on capacity of x-rays to emit core electrons from an atom. This process is known as Moseley's Law, which shows that as the frequency of light released increases, the atomic number of atom also increases. When the electron leaves the system, a hole will be created. This hole gets occupied by a higher energy electron, which releases energy as it gets relaxed [128]. The energy released is characteristic to each element in periodic table, which can be used to identify element as well as their proportion. It consists of three major parts.

- Emitter
- Collector
- Analyzer

These parts are connected to SEM, or TEM. Combining three pieces gives information about how many x-rays are released and energy associated with it.

3.9 Electrochemical Characterization

As the prepared electrodes were characterized by using XRD for crystal structure, SEM and EDX for morphology, TEM, FTIR and Raman spectroscopy for functional groups. Electrochemical analysis was used to check the water splitting applications of electrode material by performing following tests CV, LSV, EIS and Chrono-potentiometry. For this testing three electrode assembly is used which consists of reference electrode, working electrode and counter electrode. Reference and counter electrode is made of Ag/AgCl and Pt and working electrode is made by depositing catalyst on nickel foam. Preparation of working electrode consist of three steps, in first step Ni foam was treated. For the treatment of Ni foam, it sonicated with 1 M HCL solution for 30 minutes followed by Ethanol and DIW. After treatment Ni foam is dried in vacuum oven for 3 hrs at 70^{o}C. In second step Ink was prepared by adding 4-5 mg active material in 80µl Ethanol and 20µl Nafion as binder then sonicate it for 6 hours. In third step Ink was deposited on treated Ni foam and followed by overnight drying at 80^{o}C in vacuum oven. Then all the prepared electrodes are tested at different scan rates.

3.9.1 Cyclic Voltammetry (CV);

CV provides versatility and ease in inquiring about electrochemical species. It has extensive use inorganic chemistry, inorganic chemistry, biochemistry, and electrochemistry. The potential of effectiveness for CV lies in its capability to scan rapidly and observe redox reaction over catalytic surfaces. Steps involve in CV is shown in **Fig. 14** The CV apparatus relies of potential cycling on an electrode that was dipped in acidic or basic solution. The potential is caught on working electrode. Reference electrode provides control over potential coming toward working electrode. These potentials create an exciting signal which is plotted in cycles onto the graph. In this way a cyclic voltammogram is produced which presents current measure during voltage scan. CV graph is the plot of current produced against the potential applied towards the electrode. The scan starts with negative cycle, calculating parameters of reduction and then starts positive cycle for oxidation reactions [103]. A schematic diagram of CV is shown in **Fig. 15** along with its graph.

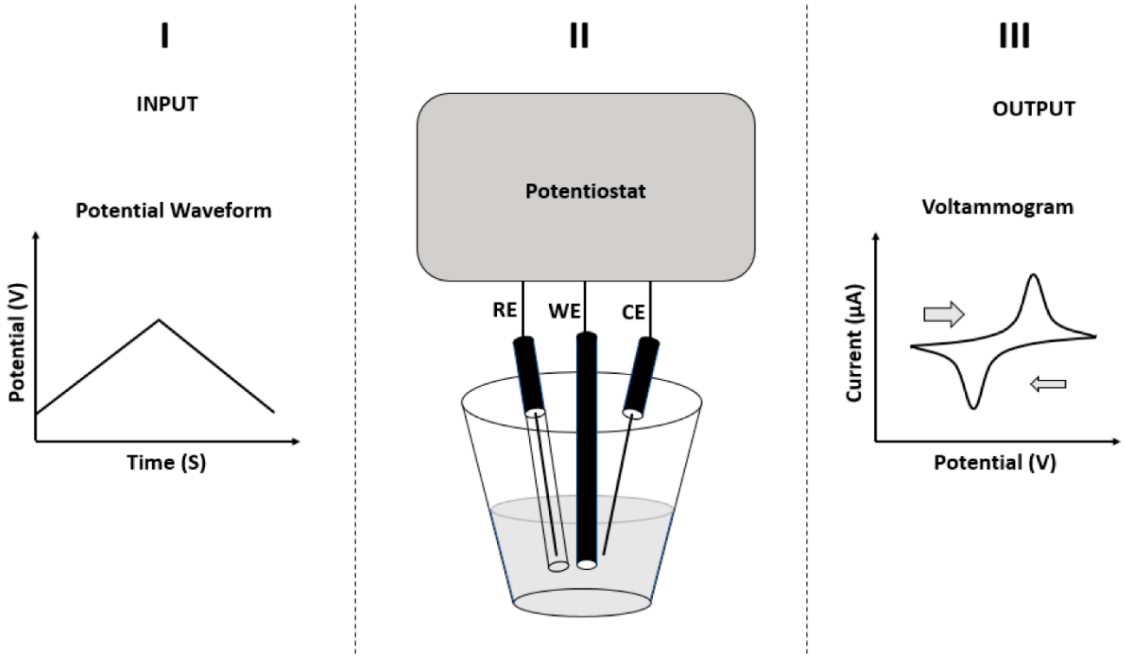

Figure 14; *Steps involve in cyclic voltammetry*

In Voltammogram, during forward scan the highest peak is oxidation peak and it corresponds to anodic current and anodic potential. Whereas, during reserve scan the peak where rate of reduction is highest is known as reduction peak and it corresponds to reduction current and reduction potential. The shape of the curve depends whether the process is reversible or irreversible.

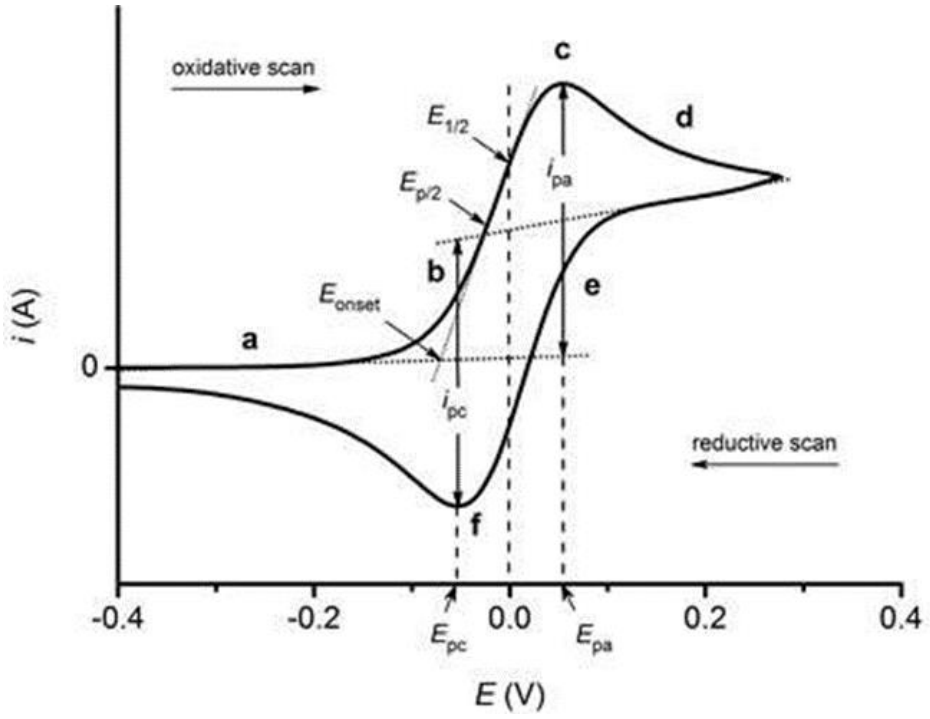

Figure 15: *Schematic of Cyclic voltammetry*

- The current peaks separate by voltage of $\Delta E = E_p^a - E_p^a$
- When scan rate changes, peak voltage position remains the same
- The ratio of the peak current gives the value of one

  $$\frac{i_p^a}{i_p^c} = 1$$
- The current peaks are directly related to the square root of the scan rate.

3.9.2 Linear sweep voltammetry

The Linear sweep voltammetry technique comprises of a fixed potential range, which is applied in a similar way as potential step measurement. The voltage scanning is performed from lower to upper limit as given below. Schematic representation of LSV is given below in **Fig. 16**

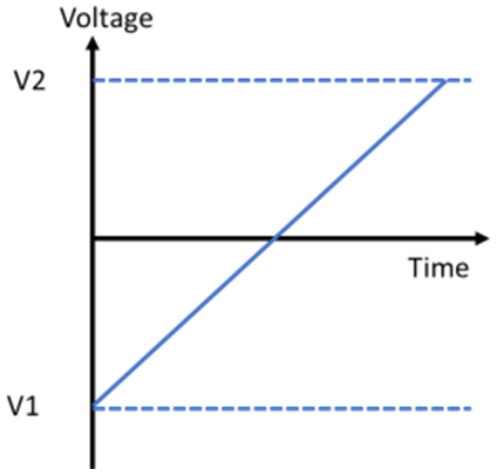

Figure 16: *Schematic representation of LSV*

The scan rate can be calculated from slope of the line. It depends on time required to sweep the voltage range. The characteristics of LSV curve depends on many factors.

- Reaction rate required to transfer an electron
- The chemical reactivity of species that are electroactive
- The voltage scan rate

The response of current is plotted against voltage.

3.9.2.1 Tafel slope

The slope of the Tafel is used for the purposes of gaining a better understanding of the Tafel behaviour of electrocatalysts and reactants. The Tafel equation could be changed into log functions. Where a low Tafel slope indicates efficient kinetics of electro

catalyst which corresponds to smaller overpotential with quick increase in current density. Tafel slope also provides an insight to OER mechanism, pointing out to the rate calculating step. Intrinsic rate of electron transfer among electrode and analyse can be directly reflected by exchange current density (J_o). However, due to the complexity of the OER mechanism and the extensive errors related to exchange current density estimation J_o, it is rarely used in OER and HER,

$$\eta = b.log\frac{j}{j.}$$

Where;

η= Over potential b= Tafel slope

j= Current density j. = exchange current density

3.9.2.2 Overpotential;

Overpotential is applied for the purpose of propelling the processes of electron transfer at a required rate which has been subjected to inactivity due to the high activation energies. This is done in order to form reaction intermediates with effectiveness, which is necessary for the configuration of reaction intermediates with effectiveness. Under the conditions that, water is at 25^{o}C and pH = 0 then according to Nernst equation,

$$E_{eq} = NHE = \frac{RT}{NF} = \ln\left(\frac{ox}{Red}\right)$$

Where,

E_{eq}= potential under equilibrium conditions

R=Ideal gas constant

T=temperature in Kalvin

N=number of moles of electrons

F= Faraday Constant

[Red]= concentration of reduced molecules

[Ox]=concentration of oxidized molecules

The required potential for electrolization of water will be Eeq = 1.23V vs. NHE.

With the change of pH, the electrode potential changes, which in turn utilizes reversible hydrogen electrode (RHE) as a reference potential at a given temperature of 25°C.

$$E_{eq}\,(RHE) \;=\; E\;\; eq\,(RHE) \;+ 0.059\,pH \;= 1.23V$$

The cell potential given as E is

$$E(RHE) = E_{Test} + E^{o} + 0.059\,pH,$$

Where

E_{RHE}=converted cell potential

E_{Test} = applied cell potential

E^{o} = cell potential at standard conditions

For different overpotential values there will be different current values accordingly. The overpotential value was commonly used as criterion at a current density of J=10 mA cm^{-2}

(η_{10}). The smaller the value of η10 more improved will be the electrolytic ability.

$$\eta \;=\; E(RHE) \;-\; E_{eq}(RHE)$$

3.9.3 Electrochemical Impedance Spectroscopy (EIS)

Electrochemical impedance spectroscopy is used to measure resistance and capacitance properties of catalyst, when an AC excitation signal is applied at 10 mV. The resistance and capacitance values are calculated by measuring in-phase and out-phase responses of current. It also provides an insight to electrochemical reactions occurring at anode and cathode. The ohmic resistance, charge transfer resistance, and diffusion transfer resistance are some of the terminology that are used to assess the internal resistance. The measurements are performed in a potentiostat with an AC amplitude of 10 mV over a frequency range of 100 kHz to 1 MHz. The frequency range of the measurements is as follows: The frequency response analyzer has the capability of recording the fluctuations in current response in addition to the voltage response. Graphical representation is given below in **Fig 17**;

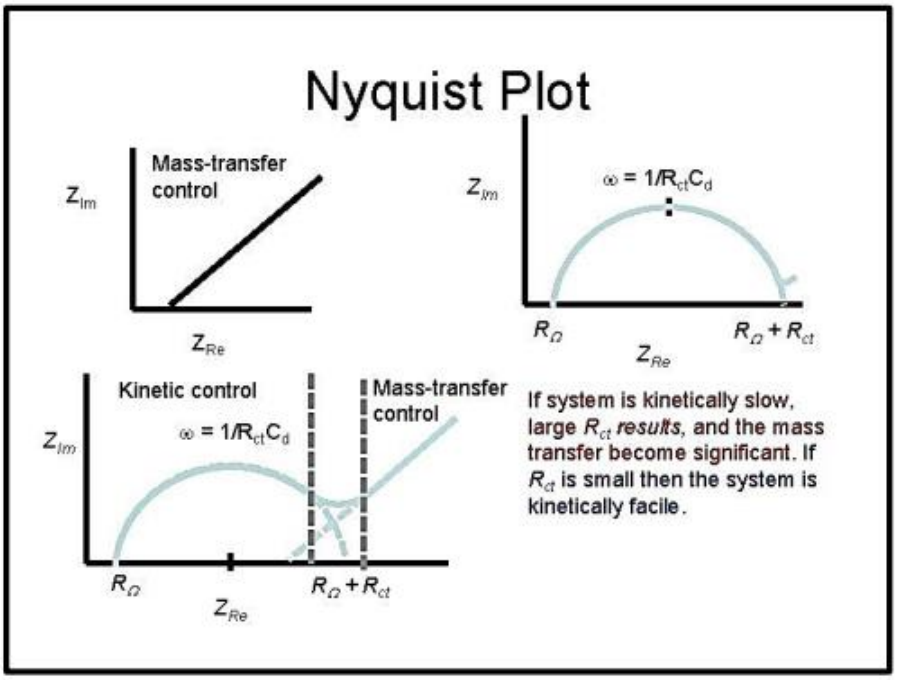

Figure 17: *Graphical Representation of Electrochemical impedance spectroscopy*

The Nyquist plot or the Bode plot can be used to represent the EIS values. When drawing the Nyquist plot, negative imaginary impedance values are plotted along the x-axis, while real impedance values are plotted along the y-axis. The data for low and high frequency are presented via the Bode plot. The value of R_p can be determined by taking the difference in resistance between low frequency and high frequency. For the purpose of demonstrating the diffusion mechanism, the Warburg element is connected in parallel to R_s and R_p in order to create an equivalent circuit[104]. Schematics of EIS is given below in **Fig. 18**

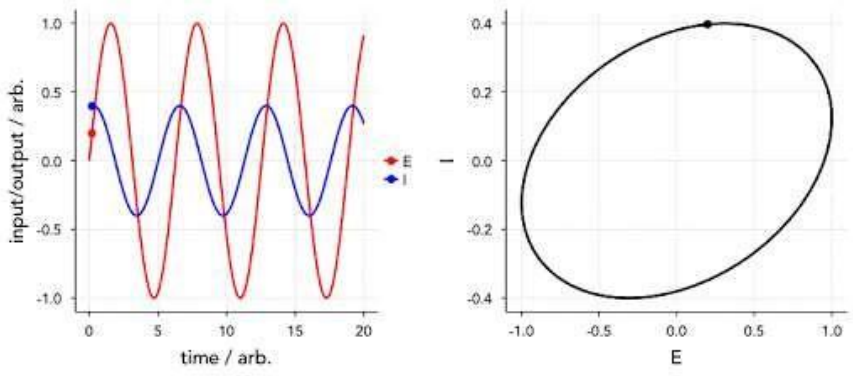

Figure 18: *Principle of Electrochemical impedance spectroscopy.*

3.9.4 Stability Test

The stability of electrocatalysts is an important activity parameter that is connected to OER catalysis. There are multiple ways in which this stability can be assessed. The cyclic stability is determined by the difference in linear sweep voltammetry (LSV) after one thousand cycle voltammetric scans have been carried out. It is also possible to show it using a durability test, which measures the change in performance over time at a particular current density (chrono-amperometry) or at a particular applied potential (Chrono-potentiometry). Both of these tests are performed at a constant applied potential. It operates by maintaining either a galvanostatic or potentiostat phase for an extremely extended period of time. If the activity of the material does not change after being subjected to such prolonged polarisation, then we may say that it is stable.

Chapter No 4

Result and Discussion

4.1 Characterization of LSTN

4.1.1 X-Ray Diffraction Analysis of LSTN

The crystallinity of synthesis electrodes was confirmed by using XRD and is given in **Fig. 19**. The XRD of prepared LSTN shows specific peaks at 22.76°, 32.46°, 39.94°, 46.50°, 52.40°, 57.84°, 67.89°, 72.65°, 77.32°, which relates directly to a crystal plane of (100), (110), (111), (200), (210), (211), (220), (221), and (310). A-site is inhabited by La and Sr, whereas B-site is shared by Ti and Ni (JCPDS No: 01-079-0181). In contrast, e-LSTN exhibited a more dramatic Ni peak impact.

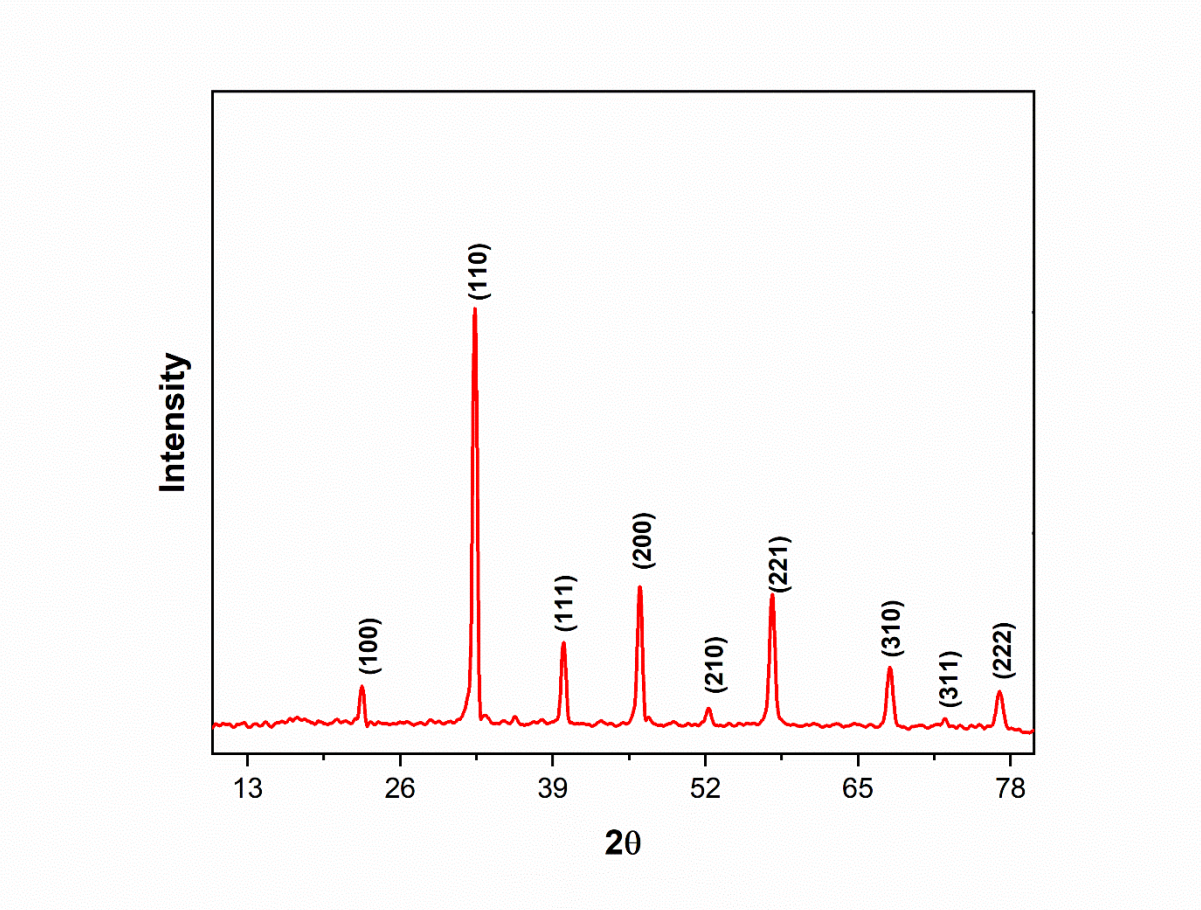

Figure 19: *XRD graph of e LSTN*

4.1.2 Scanning Electron Microscopy (SEM)

The SEM image showed in **Fig. 20** describes the erratically formed clusters of LSTN perovskite. The clusters are the tiny particles of LSTN aggregates, and their typical

dimension is less than 70 nm. These clusters create porosity channels that make it easier for electrolytes to move about. During the charge transference these interconnecting particles are very useful. Compared to macro pores, microspores facilitate the adsorption and desorption of electrolytes and provide numerous active sites for redox reactions[105]. The Ni particles get more exposed after exsolution, thereby facilitating the electron/ion diffusion and its contact with electrolyte. This has significantly increased the electrode surface area and efficiency of catalyst. Very small Ni nanoparticles of approx. 30 nm have been observed.

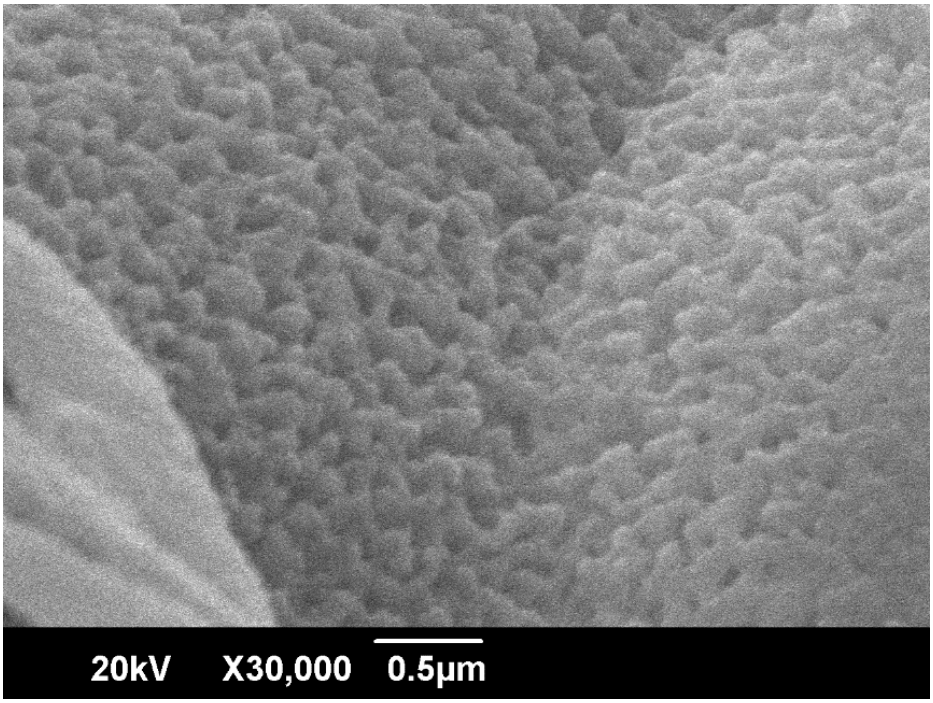

Figure 20: *SEM image of LSTN*

4.2 Characterization of g-C_3N_4

4.2.1 X-Ray Diffraction Analysis of g-C_3N_4

The crystallinity of synthesis of electrode is confirmed by the using XRD as given in **Fig 21**. The XRD pattern of pure g-CN shown in the figure below reveals a characteristic peak at 13.2° on the (100) diffraction plane. The computed inter-planar spacing is 0.67 nm with respect to JPCDS No. 87-1526. The inter-planar spacing is the distance between aromatic repeating blocks inside a single sheet. The dominant peak in this pattern occurs at 27.2°which correspond to the typical (002) plane of carbon. The sharpness of the reflection peak reveals the dense packing of sheets present in graphitic carbon nitride with strong interactions between their layers.

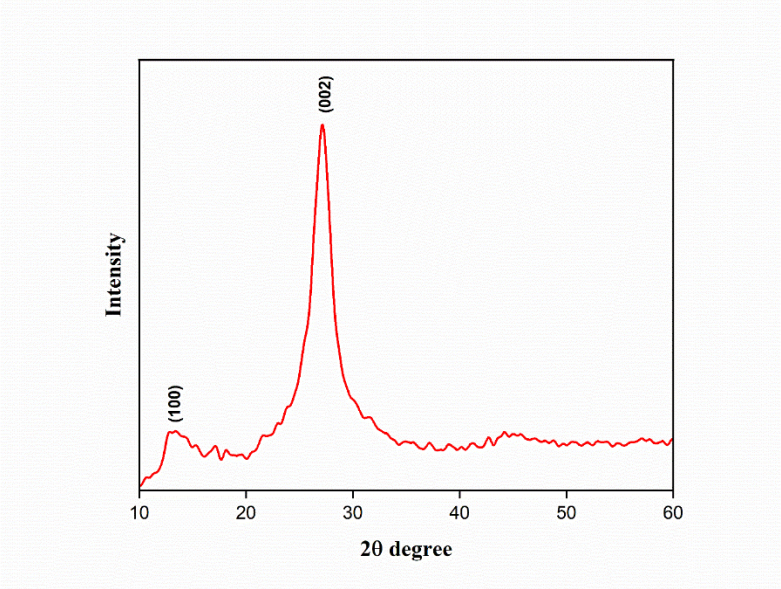

Figure 21: *XRD of g-C_3N_4*

4.2.2 Scanning electron microscopy (SEM)

Scanning electron microscopy used to check the morphology of g-CN. The g-C_3N_4 prepared by urea having small lamella and loose structure. **Fig. 22** shows that nano sheets are unevenly stacked or piled to generate flake-like shapes[106].

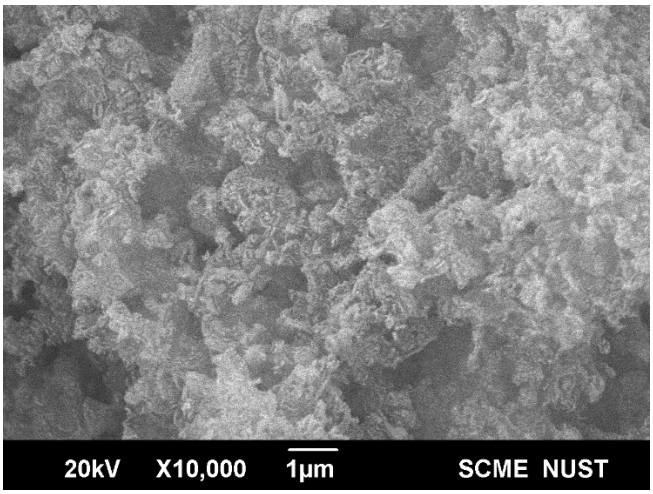

Figure 22: *SEM image of g-C_3N_4*

4.3 Characterization of LSTN, g-CN, and LSTN/g-CN Electrocatalyst

4.3.1 X-Ray Diffraction Analysis of LSTN/g-CN Electrocatalyst

The crystallinity of synthesis of electrode is confirmed by the using XRD as given in **Fig. 23**. In order to verify the creation of the g-C_3N_4 @LSTN nanocomposite, the

individual diffraction peaks of LSTN powder and g-C_3N_4 were used as a reference. The heterostructure displayed XRD peaks at 22.76°, 32.46°, 39.94°, 46.50°, 52.40°, 57.84°, 67.89° and 72.65°. These peaks correspond to the planes (100), (110), (111), (200), (210), (211), (310) and (222). While the g-C_3N_4 phase is indicated by the peaks at 13.2° and 27.2° which correspond to the planes of (100) and (002) respectively in hybrid material. The development of hybrid nanostructures has been demonstrated by the presence of distinct phases from both parent materials at the same time (LSTN and g-C_3N_4.) However, planes of LSTN such as (110), (310) and (222) were not seen in the g-C_3N_4 @LSTN nanocomposite. This can be attributed to the complex and randomly layered g-C_3N_4 on the LSTN particles, which resulted in decreased signal intensity for the planes (110), (310) and (222). In addition, the diffraction peaks for pure g-C_3N_4 are substantially wider than those of LSTN. This can be related to the relatively low crystallinity of g-C_3N_4 in comparison to that of LSTN. In addition, the absence of more peaks suggests that the pure phase g-C_3N_4 layers are successfully developed on LSTN particles by utilizing the simple sol-gel process without the addition of any contaminants.

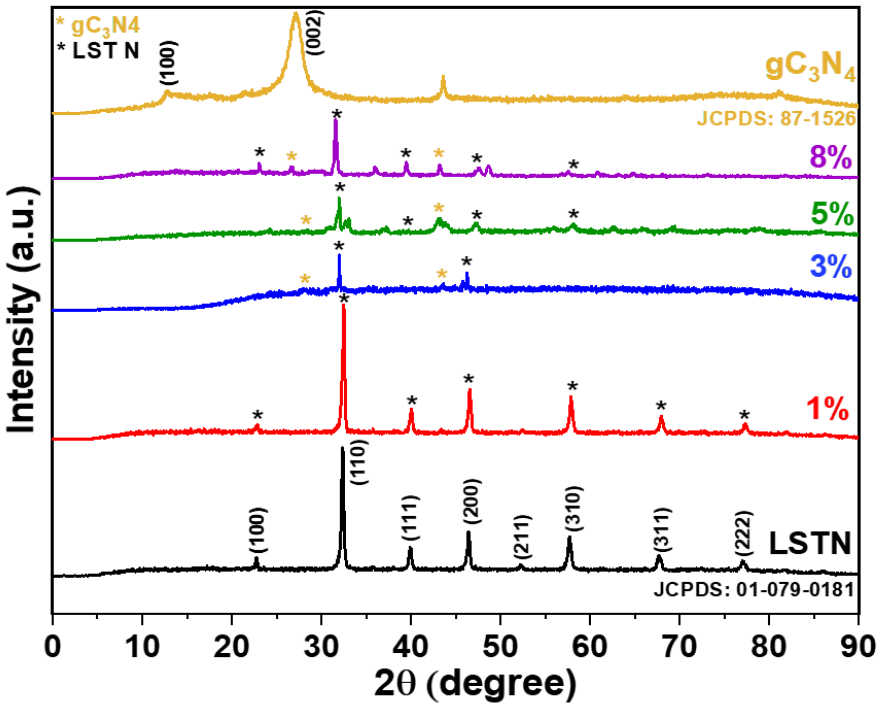

Figure 23; *XRD of LSTN,g-C_3N_4, LSTN/g-C_3N_4 hybrids*

4.3.2 Fourier Transform Infrared Spectroscopy (FTIR)

To perform additional research into the structural properties of the composite, the technology known as Fourier Transform-infrared (FT-IR) was utilised. This allowed to find the functional groups present in the compound. As can be seen in **Fig. 24**, the vibrational frequency of the metal oxide bands falls between 400 and 700 cm^{-1}. The NH_2 stretching vibration has been discovered as having intense peaks at 3400cm^{-1}. The peak at 1446 cm^{-1} correspond to C-N and the peak at 1630 cm^{-1} correspond to C=N vibrations. These peaks are the evidence of g-C_3N_4 presence in the composite. At a frequency of 1020 cm^{-1}, a peak is present which corresponds to the presence of $SrTiO_3$. Even though the peak at 800 cm^{-1} indicates a metal-oxygen bond and the Ti-O stretching vibration shown by TiO_2 supports the production of brucite type layers on LSTN particles. In other words, the presence of SrTiO3 and Ti-O stretching vibration can be inferred from the fact that these peaks come from LSTN particles. It is essential to keep in mind that every FTIR peak occur at different wavelengths that indicates the presence of specific functional group in the synthesized catalyst. The FTIR of hybrid shows the presence of functional groups from both LSTN and gC_3N_4 that confirms the formation of composite material.

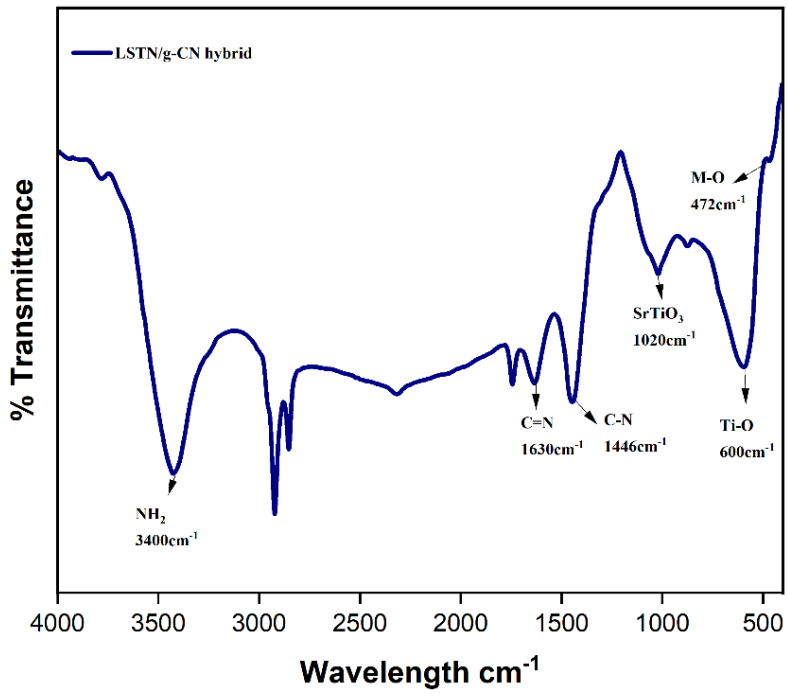

Figure 24: *FT-IR analysis of LSTN/g-C_3N_4 hybrid*

4.3.4 Scanning Electron Microscopy (SEM) of Hybrid

SEM is an outstanding technique for observing the surface of material and provides excruciate details about surface projections. It provides information about texture (external morphology) chemical composition orientation and crystalline structure. It generates an image of a material by the employment of an electron beam, and the magnifications are accomplished with the application of electromagnetic fields. Images obtained using scanning electron microscopy (SEM) of hybrid material are presented in the **Fig. 25**. The morphology of these images agrees with the research that was previously stated. The figures show SEM images for the hybrids at a variety of resolutions. Based on the synthesis of the hybrid, it is hypothesized that both components are interconnected with each other; hence, it is not possible to see a single morphology that is specific to either molecule. This method of chemical synthesis results in the creation of porous material, and the average crystallite size of hybrids is diminished as a result of particles collision. The lightning-fast current response offered by this Nano material is made possible by the one-of-a-kind synergistic action and the high activity of the materials due to its unique morphology. As can be seen in Figure, the morphological pattern of gC_3N_4@LSTN exhibits a conventional porous structure that is painted consistently in a very thick pattern on the substrate. As can be observed clearly from SEM images, it looks like nanoparticles were incorporated in sheet like structure. The effective prevention of packing and self-aggregation is achieved through the homogenous anchoring of gC_3N_4 onto the surface of LSTN perovskite. The heterostructure composite has the potential to provide a high specific surface area having porous characteristics. This helps to facilitate the flow of electrolyte towards complete Nano sheets, which ultimately leads to good catalytic performance. An image of the hybrid that has been magnified reveals that it has a petal-like structure, similar to that which is displayed by hydrangea and has a normal diameter of 1 μm. There are a number of gaps between each individual petal, and these crevices provide a variety of routes for the entry of electrolyte ions as well as mass movement. The hydrangea-type design is made up of curled sheets that are 25 nm thick and have an air gap that is 200 nm between each pair of sheets. It is the ultrathin character of the highly orientated layered composite crystal structure that is responsible for the remarkable catalytic performance that can be observed.

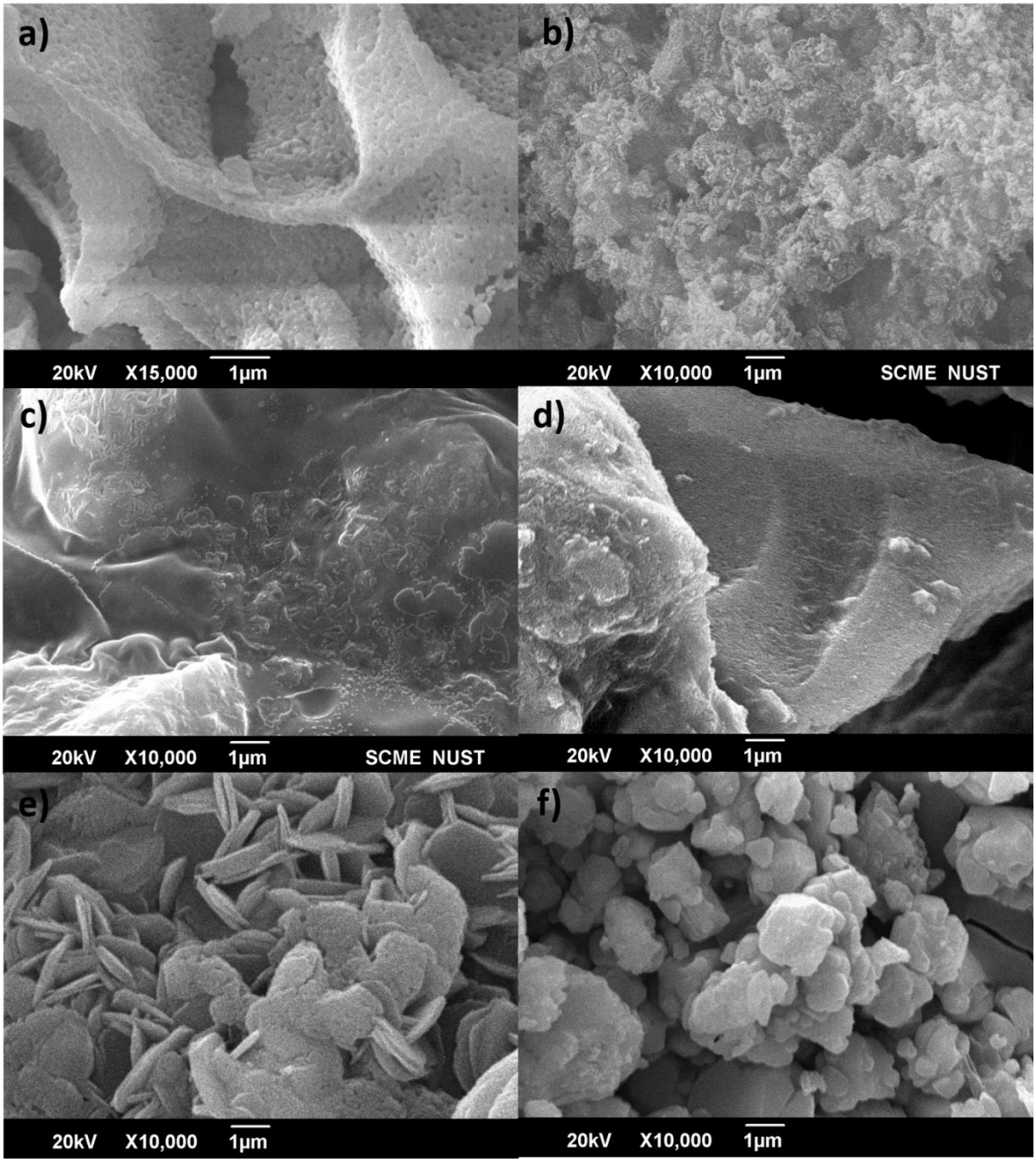

Figure 25: *SEM image of LSTN, g-C_3N_4 and their hybrids at different resolutions*

4.3.5 Energy-Dispersive X-ray Spectroscopy of Hybrid

The Energy-dispersive X-ray spectroscopy (EDX) examination that was undertaken for further investigation represents that the as prepared nanocomposite predominantly comprises of La, Sr, Ti, Ni, N, C and O elements; this, therefore, implies that the successful creation of hybrid of LSTN and g-CN has taken place. Coating of Strontium and Nickel elements into LSTN's A-site (La) and B-site was carried out successfully, as evidenced by the high intensity signal for both of these elements. The presence of

a large nickel fraction is the result of a substrate composed of nickel, along with the element's presence in heterostructure. The atomic percentages of the components g-CN@LSTN are shown in figure below in the following section. The energy-dispersive X-ray (EDX) mapping of hybrid materials that was performed to identify the homogenous presence of all of the important components, including lanthanum, strontium, nickel, titanium, carbon, nitrogen and oxygen, with ratios displayed. It is important to note that the composition did not change at any point in time. The EDX elemental graph offers further evidence that the successful creation of hybrid material gC_3N_4@LSTN was achieved.

4.4 Electrochemical Testing of LSTN, g- C_3N_4 @LSTN, and g-C_3N_4 for OER and HER

4.4.1 Linear Sweep Voltammetry Results for OER

The LSV technique comprises of a fixed potential range, which is applied in a similar way as potential step measurement. The voltage scanning is performed from lower to upper limit. It depends on time required to sweep the voltage range. The characteristics of LSV curve depends on many factors i.e., Reaction rate required to transfer an electron, the chemical reactivity of species that are electroactive, the voltage scan rate. In this, the response of current is plotted against voltage. To carry out electrochemical tests, a three-electrode assembly consisting of three electrodes is required. One of the electrodes is known as reference electrode that is usually Ag/AgCl, the second electrode is Pt wire which is used as counter electrode. The third one is our working electrode that consist of our catalyst deposited on Ni foam. The electrolyte used was the solution of 1 M KOH. It was possible to assess the HER performance by using the polarization curves of the LSV. To determine the effect of g-C_3N_4 over LSTN, all the catalysts were evaluated under the same conditions. The **Fig. 26** demonstrates the polarization curves for OER that represents the peak of oxidation at a potential of 1.38 V, which correlates with the oxidation of Ni in them. When the potential is more than 1.52 volts, there is a rapid increase in the anodic current density. Linear sweep voltammetry (LSV) demonstrates that there is a significant difference between the activities of 1wt% g-C_3N_4@LSTN, 3wt% g-C_3N_4@LSTN, 5wt% g-C_3N_4@LSTN, 8wt% g-C_3N_4@LSTN and g-C_3N_4. Perovskite's bifunctional activity is significantly enhanced by doping at both the A site (Sr) and B site (Ni) of the perovskite crystal structure. Doping with strontium results in the formation of many oxygen vacancies,

which in turn increases the number of possible pathways through which oxygen ions can move [107]. Furthermore, the presence of numerous Ni^{3+} on the surface can be attributed to the oxygen vacancies that were provided by the Ni doping, which in turn improved the catalytic activity. Despite this, the OER activity of LSTN is significantly lower than that of perovskites based on cobalt [108]. As a result of this, there is a pressing requirement to enhance OER by developing composite catalysts that are applicable in a variety of contexts. The electrochemical performance of the electrode can be significantly improved by making hybrids of LSTN. This improvement is made possible by using g-C_3N_4. It provides heterogeneous pathways for the rapid transportation of ions between the interface of electrode and electrolyte, hence improving the electrodes' overall electrochemical performance [109].

To evaluate the OER performance of all the synthesized electrocatalysts, anodic current and overpotential values at 1.6 V were also determined. This demonstrates that 3wt% g-C_3N_4@LSTN only needs a 62 mV overpotential in contrast to LSTN and g-C_3N_4, which have shown a relatively large overpotential of 76mV and 178 mV respectively than composite material. The overpotential of these catalysts for OER is given below in **table 2**.

Table 2: *Overpotential for OER*

Sr. No.	**Catalysts**	**Overpotential at 10 mA cm^{-2}**
1	LSTN	76 mV
2	g-C_3N_4	178 mV
3	1wt% g-C_3N_4 @ LSTN	74 mV
4	3wt% g-C_3N_4 @ LSTN	62 mV
5	5wt% g-C_3N_4 @ LSTN	66 mV
6	8wt% g-C_3N_4 @ LSTN	67 mV

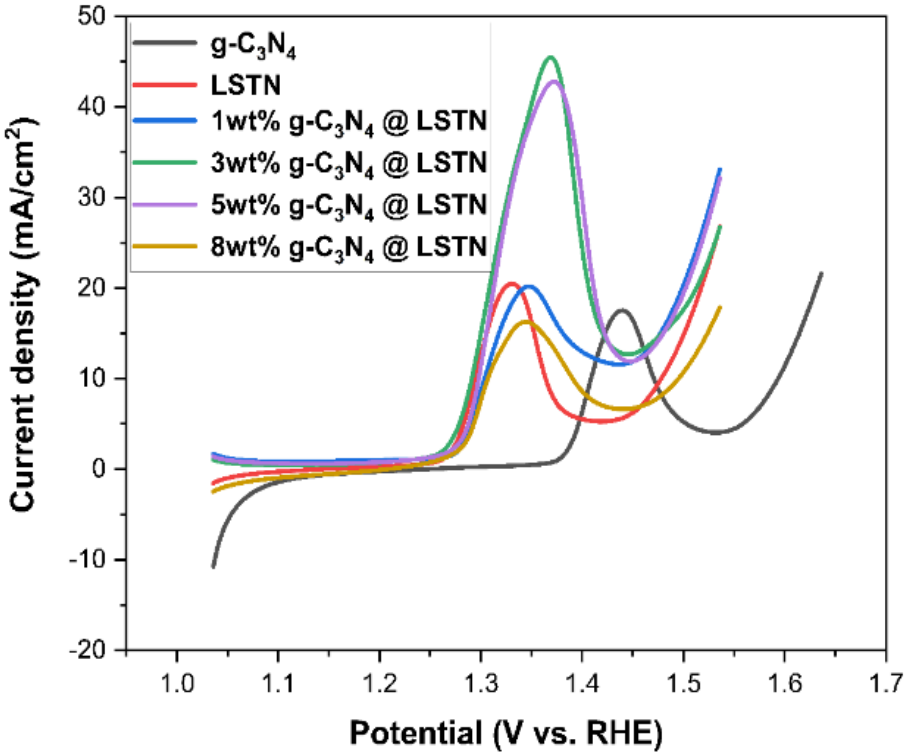

Figure 26: *Overpotential for OER*

The Tafel equation can be transformed to log functions, where a low Tafel slope indicates efficient kinetics of electro catalyst which corresponds to smaller overpotential with quick increase in current density. Tafel slope also provides an insight to OER mechanism, pointing out to the rate determining step [110]. Tafel slope for OER of these catalysts is given below in **table 3**. The relatively low Tafel slope of 3wt%g -C_3N_4@LSTN (119 mV dec^{-1}) as compared to LSTN (161 mV dec^{-1}) 1wt%g-C_3N_4@LSTN (142 mV dec^{-1}), 5wt%gC_3N_4@LSTN (129 mV dec^{-1}), 8wt% g-C_3N_4@LSTN (133 mV dec^{-1}) and g-C_3N_4 (177 mV dec^{-1}) that are depicted in **Fig. 27** is an indication of the fact that the 3wt% g-C_3N_4@LSTN is a very good electrocatalyst for OER water splitting. It has a greater electrocatalytic performance capacity than other materials due to the fact that the rate of this electrocatalyst enhances when there is an enhancement in potential. This extraordinary behaviour can be explained by a large array of oxygen species that have been adsorbed and their interaction with heterostructure catalysts on the cation sites of transition metals.

Table 3: *Tafel slop for OER*

Sr. No.	Catalysts	Tafel slopes $mVdec^{-1}$
1	LSTN	161
2	g-C_3N_4	177
3	1wt% g-C_3N_4 @ LSTN	142
4	3wt% g-C_3N_4 @ LSTN	119
5	5wt% g-C_3N_4 @ LSTN	129
6	8wt% g-C_3N_4 @ LSTN	133

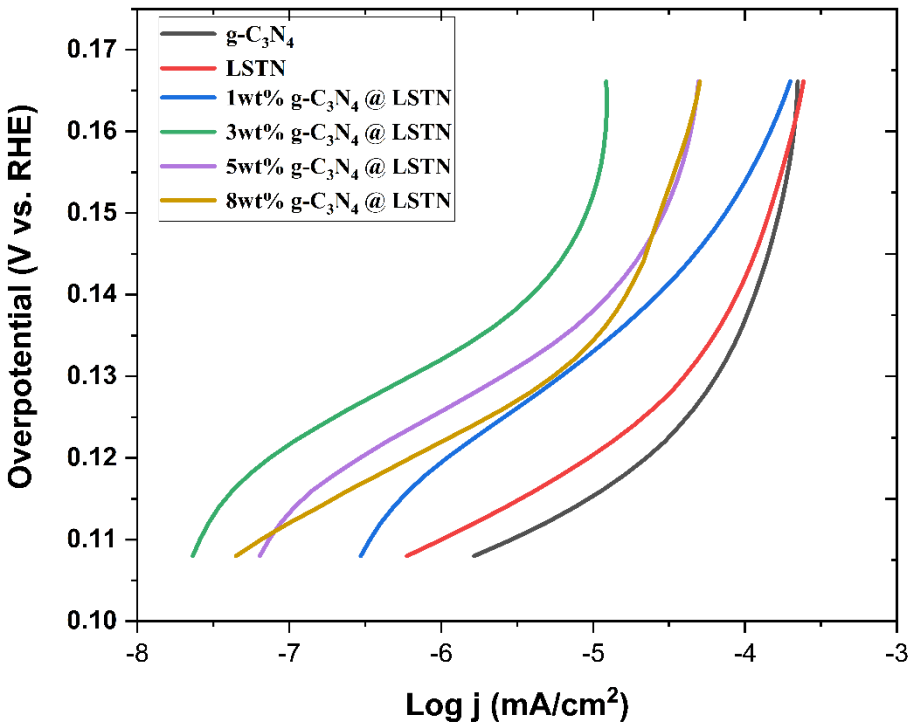

Figure 27: *Tafel slope for OER*

4.4.2 Linear sweep voltammetry results for HER

To carry out electrochemical tests, a three-electrode assembly consisting of three electrodes is required. One of the electrodes is known as reference electrode that is usually Ag/AgCl, the second electrode is Pt wire which is used as counter electrode. The third one is our working electrode that consist of our catalyst deposited on Ni foam. The electrolyte used was the solution of 1 M KOH. It was possible to assess the HER performance by using the polarization curves of the LSV. To determine the effect of g-C_3N_4 over LSTN, all the catalysts were evaluated under the same conditions. The composite g-C_3N_4@LSTN has a well-deserved reputation for being an outstanding catalyst for the hydrogen evolution reaction. With linear sweep voltammetry (LSV) curves in 1 M KOH, the HER activities of a variety of different electrocatalysts including LSTN, 1wt%g-C_3N_4@LSTN, 3wt%g-C_3N_4@LSTN, 5wt% g-C_3N_4@LSTN, 8wt% g-C_3N_4@LSTN and g-C_3N_4 were investigated in this study. The over potential for HER of these catalysts is given blow in **table 4**. According to **Fig. 28**, 3wt% g-C_3N_4@LSTN exhibited higher HER catalytic activity. This material required only -148mV to drive the current density of 10 mA/cm^2, which was a significant improvement above the performance of LSTN, 1wt% g-C_3N_4@LSTN, 5wt% g-C_3N_4@LSTN, 8wt% g-C_3N_4@LSTN and g-C_3N_4 materials with the overpotential values of -242mV, -235mV, -225mV, -226mV and -258mV respectively.

Table 4: *over potential for HER*

Sr. No.	Catalysts	Overpotential
1	LSTN	-242 m V
2	g-C_3N_4	-258 mV
3	1wt% g-C_3N_4 @ LSTN	-235 mV
4	3wt% g-C_3N_4 @ LSTN	-148 mV
5	5wt% g-C_3N_4 @ LSTN	-225 mV
6	8wt% g-C_3N_4 @ LSTN	-226 mV

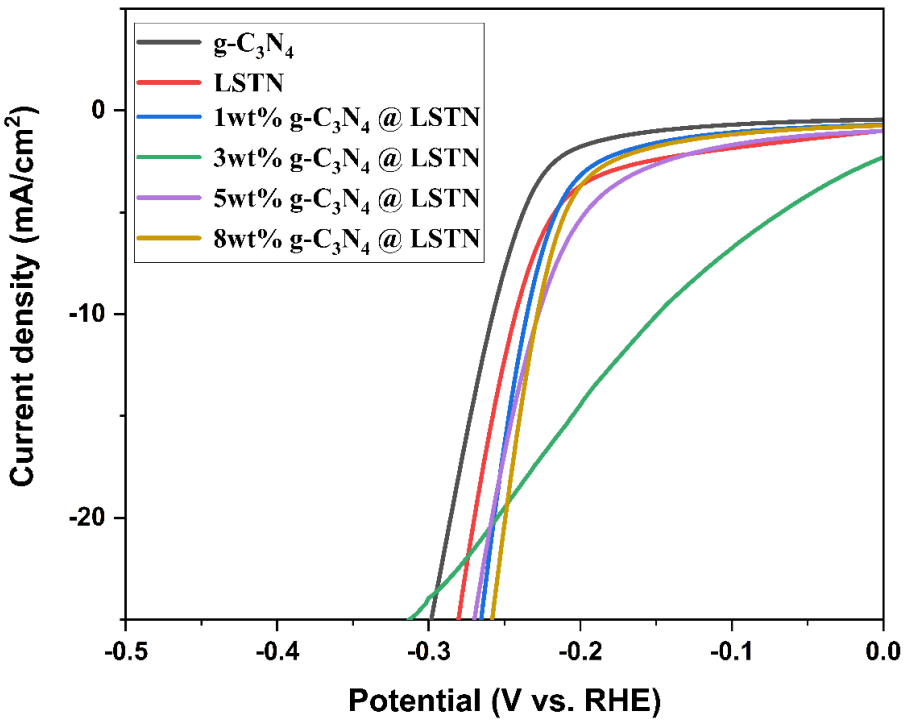

Figure 28: *Overpotential for HER*

As shown in **Fig. 29**, the corresponding Tafel plot of 3wt%gC_3N_4@LSTN has a value of 32 mVdec^{-1} that is lower than that of pure LSTN (44 mV dec^{-1}) and g-C_3N_4 (48 mVdec^{-1}) parent materials which indicates that the electrocatalytic kinetics of 3wt% g-C_3N_4@LSTN with respect to HER are superior to those of its parent materials. The Tafel slope values of all the catalysts were determined and written in **table 5**. The remarkable electrochemical behaviour of 3wt% g-C_3N_4@LSTN was achieved because of synergistic interaction among LSTN perovskites nanoparticles and g-C_3N_4, in addition to the conductive support that was supplied by Ni foam. Because of this, the adsorption of hydrogen is increased, which, together with the ordering of the phases, results in an excellent electrocatalyst. The porous nickel foam provides mechanical stability and also makes it easier for electrolytic ions to flow toward electroactive sites by offering narrower routes. This is made possible by the fact that the foam is mechanically stable [110].

Table 5: *Tafel slope for HER*

Sr. No.	Catalysts	Tafel slopes $mVdec^{-1}$
1	LSTN	44.0
2	g-C_3N_4	48.0
3	1wt% g-C_3N_4 @ LSTN	42.0
4	3wt% g-C_3N_4 @ LSTN	32.0
5	5wt% g-C_3N_4 @ LSTN	37.0
6	8wt% g-C_3N_4 @ LSTN	40.0

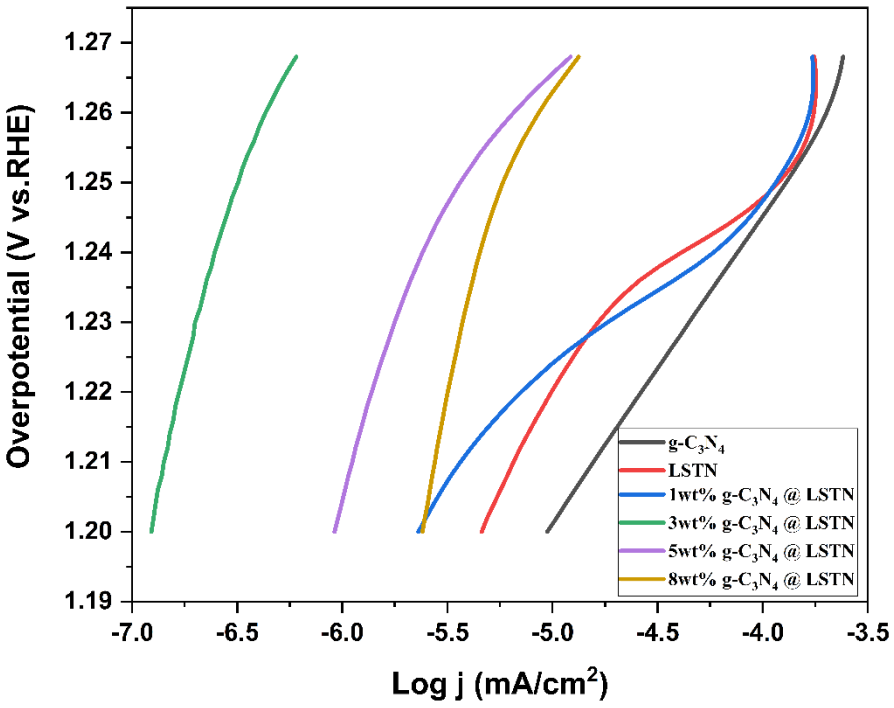

Figure 29: *Tafel slope for HER*

4.4.3 Cyclic Voltammetry

The **fig. 30** shows the cyclic voltammetric graphs of g-C_3N_4@LSTN which were studied at the scan rate from 5 to 50 mV/s. A pair of distinct redox peaks can be seen in the potential range of 0.7-1.7 V. These peaks correlate to B-type curves [110]. In addition, the adsorption of OH- at the electrode surface is the most important step in determining the reversibility of the material that makes up the electrode. The configuration of CV remains unchanged even though the scan rate is being increased; this indicates a relatively low resistance, great cyclic stability as well as exceptional catalytic performance of the electrodes. The rise in the scan rate decreases the resistance of the diffusion layer which allows for a higher current density to be achieved. In addition, nickel foam has a weak OER activity and does not contribute much to this activity. It is solely added as a semiconducting supportive material [111]. The porosity of nickel foam allows for effective flows and an easier material to work with hydrogen and oxygen departure. These peaks in redox potential are connected to reactions known as faradaic redox reactions.

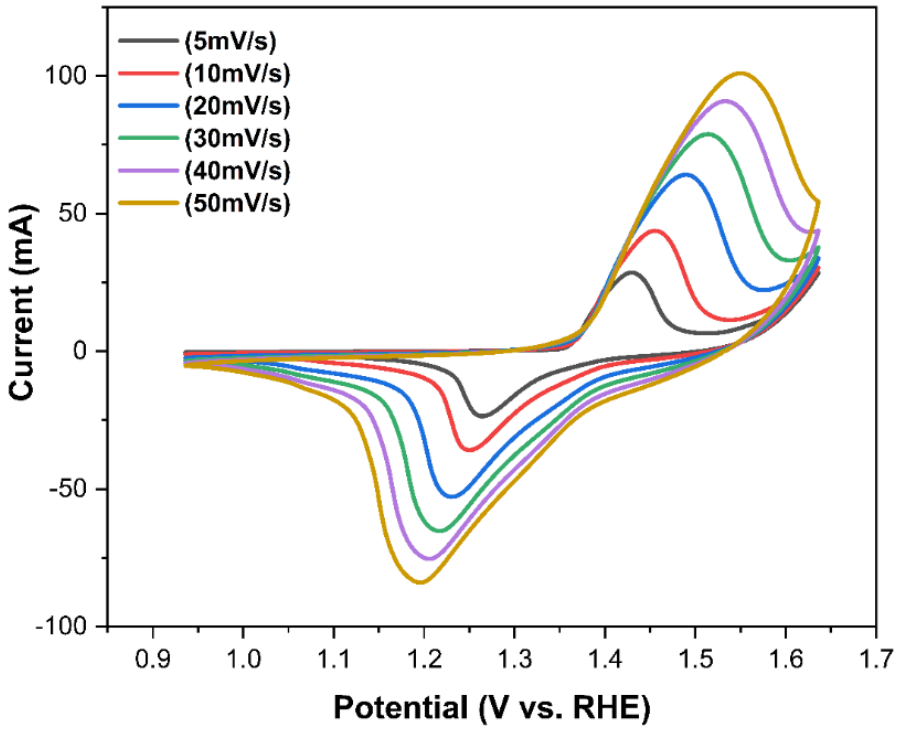

Figure 30: *Cyclic voltammetry curve for LSTN@g-C_3N_4 at a scan rate of 5, 10, 20, 40 & 50*

The cyclic voltammetry graphs of LSTN, g-C_3N_4 are shown in **fig. 31 (a-f)**. The cyclic voltammetric graphs were studied at the scan rate from 5 to 50 mV/s. A pair of distinct redox peaks can be seen in the potential range of 0.7-1.7 V. These peaks correlate to B-type curves. The comparison of CV curves for LSTN, 1wt%gC_3N_4@LSTN, 3wt% g-C_3N_4@LSTN, 5wt% g-C_3N_4@LSTN, 8wt% g-C_3N_4@LSTN and g-C_3N_4 shows clear difference in redox peaks as well as current density for the prepared composite. The LSTN, 1wt%gC_3N_4@LSTN, 3wt% g-C_3N_4@LSTN, 5wt% g-C_3N_4@LSTN, 8wt% g-C_3N_4@LSTN and g-C_3N_4 shows current in oxidation peak at 13.28mA, 33.2mA, 44.4mA, 27.2mA, 25.92mA and 13.09mA respectively at the scan rate of 5mAs^{-1}. The current value regarding reductions peaks of LSTN, 1wt%gC_3N_4@LSTN, 3wt%gC_3N_4@LSTN, 5wt%gC_3N_4@LSTN, 8wt%gC_3N_4@LSTN and gC_3N_4 is -9.9 mA, -27.1mA, -37.2 mA, -23.35mA, -22.8 mA and -13.09 mA respectively. The confirmation of the electrode's stability is provided by the fact that there is linear rise of redox peaks with scan rate as could be clearly seen from the CV polarization curves [112].

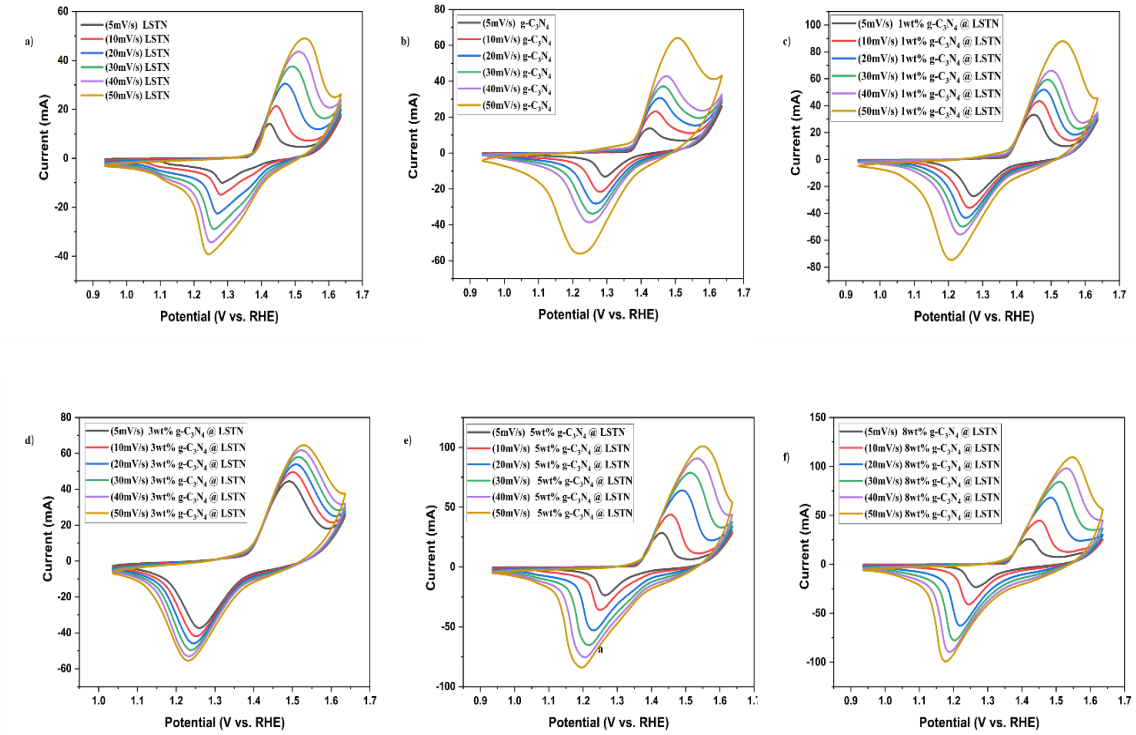

***Figure 31**: CV graphs at different scan rates 5, 10, 20,30,40,50 mV/S a) LSTN b) g-C3N4 C) 1 wt.% hybrid d) 3 wt.% hybrid e) 5 wt.% hybrid f) 8 wt.% hybrid*

4.4.4 Electrochemical Impedance Spectroscopy

To check resistance and capacitance properties of catalyst, when an AC excitation signal is applied at 10 mV, electrochemical impedance spectroscopy is used. The resistance and capacitance values are calculated by measuring in-phase and out-phase responses of current. It also provides an insight to electrochemical reactions occurring at anode and cathode. That is why, measurements were made with impedance spectroscopy to learn more about how the catalyst worked after it was synthesized [113]. The representation of EIS is shown in **fig. 32**. The EIS results of synthesized catalysts were determined within frequency range between 205 Hz and 0.1 Hz, and the experiment was done in a solution with 1 M KOH. The main purpose of EIS is to find resistance. The EIS plot is shown by a half-circle known as Nyquist plot that is used to find the resistance comes from a faradic reaction which happens at the surface of electrode [114]. It can be observed clearly from EIS plots that 3wt% g-C_3N_4@LSTN has a lower charge transfer resistance (Rct) of 9.959 e^{-3} **Ω** that is represented by the less diameter of the semicircle, which shows how well charge can be moved. The polarization resistance of LSTN has been measured to be 15.25e^{-3} **Ω**, while the polarization resistance of gC_3N_4 has been measured to be 22.86e^{-3} **Ω**. According to **Table 6**, the electrolyte resistance of the LSTN, 1wt% g-C_3N_4@LSTN, 3wt% g-C_3N_4@LSTN, 5wt% g-C_3N_4@LSTN, 8wt% g-C_3N_4@LSTN and g-C_3N_4 were measured to be 1.835**Ω**, 1.136**Ω**, 1.208**Ω**, 1.248**Ω**, 1.249**Ω** and 1.434**Ω** respectively. The decrease in the radius of semi-circle represents lower resistance value which in turn shows high charge transfer rate that is suitable for the electro-catalyst to function effectively [115].

Table 6: *EIS table for LSTN, g-C_3N_4 and hybrids*

Sr. No	Catalysts	Rct.	Ru	Cf
1.	LSTN	15.25e^{-3}	1.835	481.2e^{-9}
2.	g-C_3N_4	22.86e^{-3}	1.434	330.2e^{-9}
3.	1wt% g-C_3N_4 @ LSTN	10.79e^{-3}	1.136	966.82e^{-9}

4.	3wt% g-C_3N_4 @ LSTN	$9.959e^{-3}$	1.208	$1.348e^{-9}$
5.	5wt% g-C_3N_4 @ LSTN	$11.11e^{-3}$	1.248	$264.7e^{-9}$
6.	8wt% g-C_3N_4 @ LSTN	$13.52e^{-3}$	1.249	$488.1e^{-9}$

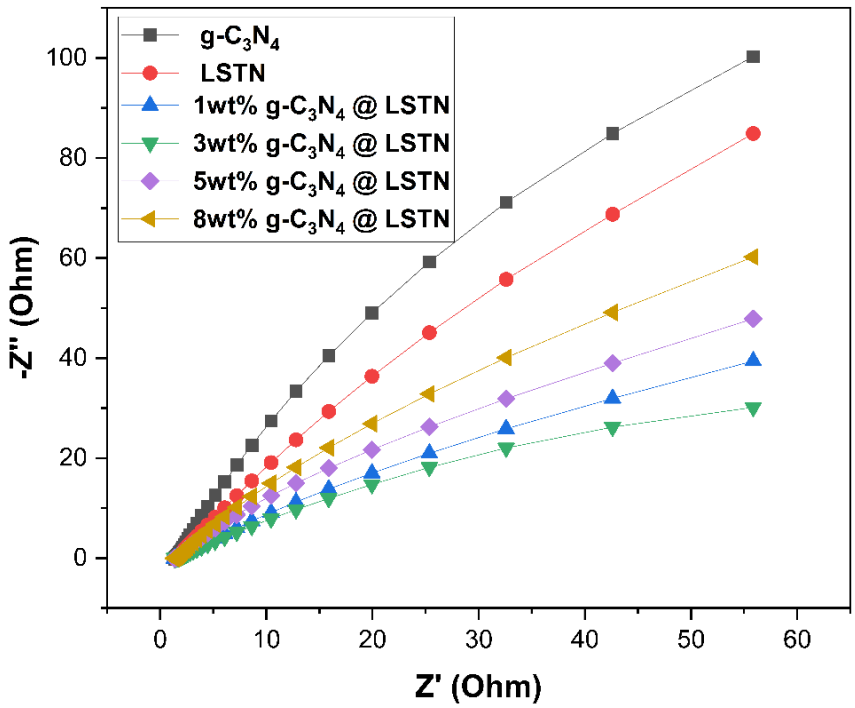

Figure 32 *The Nyquist plot for LSTN, g-C_3N_4, and LSTN@g-C_3N_4 hybrids*

4.4.5 Stability Test

The electro catalyst's stability is an essential activity parameter related to OER catalysis it can be determined in various ways. The cyclic stability depends upon the alteration in linear sweep voltammetry (LSV) after performing 1000 cycle Voltammetric scans. It can also be depicted by durability test, which is provided by the altering the performance at specific current density or at a specific applied potential with respect to time. The stability of 3wt% g-C_3N_4@LSTN was evaluated at .A for a period of two hours. The findings of Chrono-potentiometry on heterostructure have demonstrated that it maintains a consistent behaviour throughout time that could be

credited to the structure of the material. When there is a low ion diffusion resistance, it is simpler for ions to flow quickly across the active sites that are broadly exposed. This is because a good interface among the electrolyte and electrode, the causes low ion diffusion resistance. This occurs because of the synthesized material being activated while the Chrono-potentiometry test is being performed. Initially, there is a rapid response from the potential, but after some time, there is no change. There is only a difference of 0.03V in the potential. These stability results shows that the synthesized catalyst is very stable. As shown in **fig. 33** below

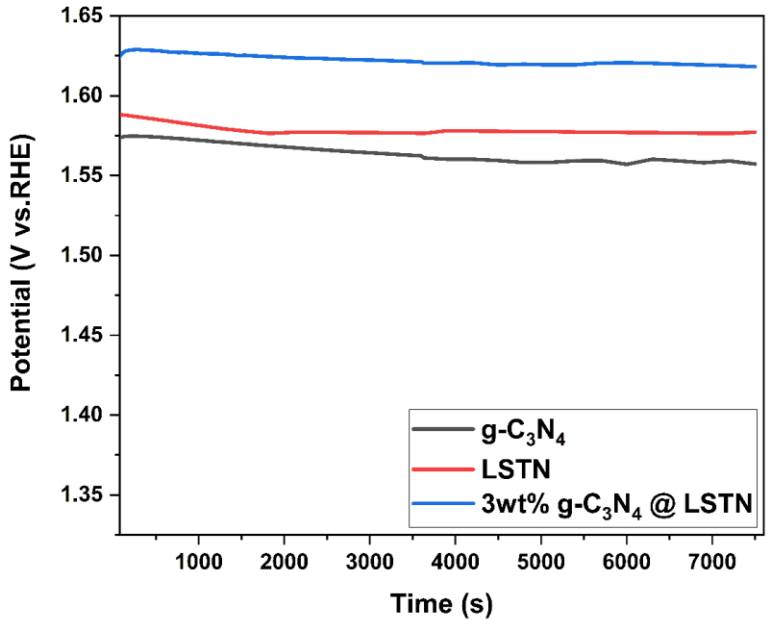

Figure 33: *Comparison of chronopotentiometry curve for g-C_3N_4, LSTN and 3wt% g-C_3N_4@LSTN for 2 hours*

Challenges for Perovskites as Bifunctional Catalysts for Water Splitting

Compared to the tremendous progress of design strategies for the improving performance of catalyst, durability has received far less interest, despite the fact that it is of greater relevance for device-based uses. The majority of perovskites experience amorphization in OER that leads to the leaching of cations from the A/B sites into the electrolyte. It was discovered that such amorphization occurred in majority and over the extremely active surface (BSCF) [64],[116] which resulted in a structural shift from corner shared octahedra towards edge shared octahedra. In addition, it was discovered that none of the catalysts, including electrocatalysts named Ni and Fe, are stable over the long term.

Even though the two half-cell reactions process had been thoroughly researched on catalysts like perovskites, optimising this catalyst remains challenging because of the process's complexity. To better understand the process of two half-cell reactions on the surface of perovskite oxide, it is required to construct a clear cut unique perovskite that interconnects the surface electrochemistry and electronic configuration of perovskite oxides. There are disadvantages associated with the stability, restricted electromagnetic efficiency, and low conductivity of pure perovskites. As a dopant, rare-earth and precious metals are utilised in perovskites with the goal of improving the perovskite crystal structure's physicochemical qualities. As a consequence, the incorporation of RE metals with changeable valence states and electronic structures leads in versatile redox characteristics as well as better electromagnetic properties. In addition, partial replacement at A/B-site cations of perovskite increases activity of catalyst but on the other hand also weakened perovskite. Additionally, the impact of synergy among the secondary component and oxide must be investigated for other hybrids perovskite electrocatalysts. To enhance the effectiveness of the perovskites as catalysts, more accessible active sites are required for cathodic and anodic activity.

The standard methods for preparing perovskite electrocatalysts are exceedingly difficult and need specialised equipment for comprehensive manufacture. For practical applications, perovskite oxides must be inhibited from undergoing structural changes in catalysis by means of such research.

Conclusion

Synthesis of LSTN perovskite using sol gel method was developed in this research incorporating CA/EDTA as binder followed by high temperature calcination. Beaker is used in this process and all the elements added in DIW. Then heated at 250 oC for 12 hours until solid powder formed. Then this solid powder put in muffle furnace in crucible at 1000oC for 10 hours. After that LSTN powder is formed. The crucible is made up of material which could bear high temperature and is inert towards almost all types of compounds to avoid contamination. As a supporting element as well as current enhancer for catalyst, graphitic carbon nitride (g-C_3N_4) was also synthesized by heating of urea at the temperature of 550^oC in muffle furnace. while heating rate was 5 degrees/min. Hybrids of g-C3N4 with LSTN perovskites of 1, 3, 5 and 8 wt.% were prepared using the same sol gel method and their water splitting applications were tested by using the electrochemical water splitting techniques.

In the end, all of the catalysts were characterised by employing various techniques such as XRD, FTIR, SEM, and EDX in order to examine the structural and morphological features. Electrochemical studies including LSV, CV, EIS and Chrono potentiometry are used to check the water spiting applications of these catalysts.

Regarding the morphology, pure LSTN perovskite has irregular flower like structure. Whereas in case of g-C3N4, layers like structure with irregular shape agglomerates can be seen. Correspondingly, hybrids of g-C_3N_4 with LSTN perovskite has proper shape crystals along with porous network like structure embedded by g-C_3N_4. LSTN@g-C_3N_4 as bifunctional catalyst shows excellent activity for both HER and OER when it deposited on highly active nickel foam. The overpotential for HER and OER is 140mV and 62 mV respectively at current density of 10 mA cm^{-2}. The future work is based on preparing double perovskites to attain highly exposed active sites and increased ion diffusion. Therefore, a B-site cation doped double perovskite has also been synthesized to achieve high bifunctional activity. The prepared catalyst has provided a new pathway to prepare bifunctional electrocatalyst.

Future Recommendations

On the surfaces of perovskites, a better knowledge of the OER, ORR, and HER mechanisms is required. The mechanisms described in the research journals require substantial experimentation to confirm their validity. Alternatively, perovskite catalyst synthesis methods require optimization. It may be able to rapidly construct active perovskite HER catalysts through integrating knowledge from reaction mechanism research with optimized catalyst synthesis. The reliance on extremely expensive and cutting-edge characterization techniques impedes further investigation of mechanisms. Therefore, the discovery of novel materials could lead to the creation of new structures and, consequently, new functionalities, some of which have been anticipated by utilizing DFT analysis. Correspondingly, for industrial applications, the lower HER is advantageous because the less value of HER with the activity of the catalyst, it may be possible to investigate the application of Separate catalysts for both OER and HER, i.e., hybrid catalysts.

In order for perovskite electrocatalysts to find broad use, one of the primary challenges that must first be overcome is the issue of the operational stability of the perovskite catalysts. As we have gone over in great detail, the stated stability tests in the recent research comprise electrochemical testing that is performed over a short period of time. The alterations that take place at the electrode surfaces are extremely dynamic during the first few hours of operation. Long-term electrochemical stability investigations could be undertaken to clarify the causes for effectiveness deterioration of the perovskites electrocatalysts. This would be necessary for the development of a catalyst that is stable and could be used in commercial applications. In addition, the conditions of stability testing conducted in research labs do not meet the standards of the industrial setting. For instance, in a real electrolyzer, there is the potential for operation at a variety of voltages. The stability of the catalyst when it comes to operation at a variety of voltages is something that can also be investigated in order to gain a better understanding of the perovskite electrocatalysts' long-term application. Consequently, application-oriented research could also carried out in greater depth for extended periods of testing time at operational conditions that are of greater interest to the industrial sector. For instance, testing should take place in the current density range of 0.5–2.0 A cm2 and at a higher temperature.

Plenty of research could be done in this field to commercialize catalysts. Double perovskites, and triple perovskites are having great potential to be explored in this area. Insitu synthesis of perovskite composites with MoS2 will result in highly active HER catalyst.

References

[1]. J. A. Turner, "Sustainable hydrogen production," *Science,* vol. 305, no. 5686, pp. 972-974, (2004).

[2]. T. R. Cook, D. K. Dogutan, S. Y. Reece, Y. Surendranath, T. S. Teets, and D. G. Nocera, "Solar energy supply and storage for the legacy and nonlegacy worlds," *Chemical reviews,* vol. 110, no. 11, pp. 6474-6502, (2010).

[3]. N. S. Lewis and D. G. Nocera, "Powering the planet: Chemical challenges in solar energy utilization," *Proceedings of the National Academy of Sciences,* vol. 103, no. 43, pp. 15729-15735, (2006).

[4]. Z. W. Seh, J. Kibsgaard, C. F. Dickens, I. Chorkendorff, J. K. Nørskov, and T. F. Jaramillo, "Combining theory and experiment in electrocatalysis: Insights into materials design," *Science,* vol. 355, no. 6321, p. eaad4998, (2017).

[5]. R. Selin, "The outlook for energy: a view to 2040," (2013).

[6]. J. M. Campos-Martin, G. Blanco-Brieva, and J. L. Fierro, "Hydrogen peroxide synthesis: an outlook beyond the anthraquinone process," *Angewandte Chemie International Edition,* vol. 45, no. 42, pp. 6962-6984, (2006).

[7]. H. Ding, C. Luo, X. Li, D. Cao, Q. Shen, and L. Zhang, "Development of BaSrCo-based perovskite for chemical-looping steam methane reforming: A study on synergistic effects of A-site elements and CeO2 support," *Fuel,* vol. 253, pp. 311-319, (2019).

[8]. Y. Bu *et al.*, "A highly efficient and robust cation ordered perovskite oxide as a bifunctional catalyst for rechargeable zinc-air batteries," *Acs Nano,* vol. 11, no. 11, pp. 11594-11601, (2017).

[9]. F. Song *et al.*, "Transition metal oxides as electrocatalysts for the oxygen evolution reaction in alkaline solutions: an application-inspired renaissance," *Journal of the American Chemical Society,* vol. 140, no. 25, pp. 7748-7759, (2018).

[10]. J. Wang, W. Cui, Q. Liu, Z. Xing, A. M. Asiri, and X. Sun, "Recent progress in cobalt-based heterogeneous catalysts for electrochemical water splitting," *Advanced materials,* vol. 28, no. 2, pp. 215-230, (2016).

[11]. J. Yu, Q. Wang, D. O'Hare, and L. Sun, "Preparation of two dimensional layered double hydroxide nanosheets and their applications," *Chemical Society Reviews,* vol. 46, no. 19, pp. 5950-5974, (2017).

[12]. L. Lv, Z. Yang, K. Chen, C. Wang, and Y. Xiong, "Electrocatalysts: 2D Layered Double Hydroxides for Oxygen Evolution Reaction: From Fundamental Design to Application (Adv. Energy Mater. 17/2019)," *Advanced Energy Materials,* vol. 9, no. 17, p. 1970057, (2019).

[13]. S. Gupta, W. Kellogg, H. Xu, X. Liu, J. Cho, and G. Wu, "Bifunctional perovskite oxide catalysts for oxygen reduction and evolution in alkaline media," *Chemistry–An Asian Journal,* vol. 11, no. 1, pp. 10-21, (2016).

[14]. M. Gong and H. Dai, "A mini review of NiFe-based materials as highly active oxygen evolution reaction electrocatalysts," *Nano Research,* vol. 8, no. 1, pp. 23-39, (2015).

[15]. N.-T. Suen, S.-F. Hung, Q. Quan, N. Zhang, Y.-J. Xu, and H. M. Chen, "Electrocatalysis for the oxygen evolution reaction: recent development and future perspectives," *Chemical Society Reviews,* vol. 46, no. 2, pp. 337-365, (2017).

[16]. H. Osgood, S. V. Devaguptapu, H. Xu, J. Cho, and G. Wu, "Transition metal (Fe, Co, Ni, and Mn) oxides for oxygen reduction and evolution bifunctional catalysts in alkaline media," *Nano Today,* vol. 11, no. 5, pp. 601-625, (2016).

[17]. M. Tahir *et al.,* "Electrocatalytic oxygen evolution reaction for energy conversion and storage: a comprehensive review," *Nano Energy,* vol. 37, pp. 136-157, (2017).

[18]. T. Liu *et al.*, "Enhanced electrocatalysis for energy-efficient hydrogen production over CoP catalyst with nonelectroactive Zn as a promoter," *Advanced Energy Materials,* vol. 7, no. 15, p. 1700020, (2017).

[19]. C. Xiong *et al.*, "Nitrogen-doped carbon nanotubes as catalysts for oxygen reduction reaction," *Journal of power sources,* vol. 215, pp. 216-220, (2012).

[20]. Y. Wang, D. Yan, S. El Hankari, Y. Zou, and S. Wang, "Recent progress on layered double hydroxides and their derivatives for electrocatalytic water splitting," *Advanced Science,* vol. 5, no. 8, p. 1800064, (2018).

[21]. S. Liu *et al.*, "The synergistic effect of Ni promoter on Mo-S/CNT catalyst towards hydrodesulfurization and hydrogen evolution reactions," *Fuel,* vol. 232, pp. 36-44, 2018.

[22]. S. Hussain *et al.*, "WS (1− x) Se x nanoparticles decorated three-dimensional graphene on nickel foam: a robust and highly efficient electrocatalyst for the hydrogen evolution reaction," *Nanomaterials,* vol. 8, no. 11, p. 929, (2018).

[23]. X. Zhang, Q. Zhang, Y. Sun, and J. Guo, "Hybrid catalyst of MoS2-CoMo2S4 on graphene for robust electrochemical hydrogen evolution," *Fuel,* vol. 184, pp. 559-564, (2016).

[24]. Y. Hou, M. R. Lohe, J. Zhang, S. Liu, X. Zhuang, and X. Feng, "Vertically oriented cobalt selenide/NiFe layered-double-hydroxide nanosheets supported on exfoliated graphene foil: an efficient 3D electrode for overall water splitting," *Energy & Environmental Science,* vol. 9, no. 2, pp. 478-483, (2016).

[25]. Y. Zhao *et al.*, "Graphitic carbon nitride nanoribbons: graphene-assisted formation and synergic function for highly efficient hydrogen evolution," *Angewandte Chemie International Edition,* vol. 53, no. 50, pp. 13934-13939, (2014).

[26]. M. Tahir *et al.*, "Bifunctional catalysts of Co3O4@ GCN tubular nanostructured (TNS) hybrids for oxygen and hydrogen evolution reactions," *Nano Research,* vol. 8, no. 11, pp. 3725-3736, (2015).

[27]. Y. Gogotsi, "What nano can do for energy storage," vol. 8, ed: ACS Publications, (2014), pp. 5369-5371.

[28]. Z. Cai, X. Bu, P. Wang, J. C. Ho, J. Yang, and X. Wang, "Recent advances in layered double hydroxide electrocatalysts for the oxygen evolution reaction," *Journal of Materials Chemistry A,* vol. 7, no. 10, pp. 5069-5089, (2019).

[29]. H. Tanaka and M. Misono, "Advances in designing perovskite catalysts," *Current Opinion in Solid State and Materials Science,* vol. 5, no. 5, pp. 381-387, (2001).

[30]. J. Xu, C. Chen, Z. Han, Y. Yang, J. Li, and Q. Deng, "Recent advances in oxygen electrocatalysts based on perovskite oxides," *Nanomaterials,* vol. 9, no. 8, p. 1161, (2019).

[31]. J. Dai *et al.*, "Enabling high and stable electrocatalytic activity of iron-based perovskite oxides for water splitting by combined bulk doping and morphology designing," *Advanced Materials Interfaces,* vol. 6, no. 1, p. 1801317, (2019).

[32]. W. G. Hardin *et al.*, "Tuning the electrocatalytic activity of perovskites through active site variation and support interactions," *Chemistry of Materials,* vol. 26, no. 11, pp. 3368-3376, (2014).

[33]. W. G. Hardin, D. A. Slanac, X. Wang, S. Dai, K. P. Johnston, and K. J. Stevenson, "Highly active, nonprecious metal perovskite electrocatalysts for

bifunctional metal–air battery electrodes," *The journal of physical chemistry letters,* vol. 4, no. 8, pp. 1254-1259, (2013).

[34]. J. T. Mefford, W. G. Hardin, S. Dai, K. P. Johnston, and K. J. Stevenson, "Anion charge storage through oxygen intercalation in LaMnO3 perovskite pseudocapacitor electrodes," *Nature materials,* vol. 13, no. 7, pp. 726-732, (2014).

[35]. N. S. Arul and V. D. Nithya, *Revolution of Perovskite*. Springer, (2020).

[36]. X. Zou and Y. Zhang, "Noble metal-free hydrogen evolution catalysts for water splitting," *Chemical Society Reviews,* vol. 44, no. 15, pp. 5148-5180, (2015).

[37]. A. Lasia, "Hydrogen evolution reaction," *Handbook of fuel cells,* vol. 815, (2010).

[38]. O. Diaz-Morales, F. Calle-Vallejo, C. de Munck, and M. T. Koper, "Electrochemical water splitting by gold: evidence for an oxide decomposition mechanism," *Chemical Science,* vol. 4, no. 6, pp. 2334-2343, (2013).

[39]. Z.-L. Wang, D. Xu, J.-J. Xu, and X.-B. Zhang, "Oxygen electrocatalysts in metal–air batteries: from aqueous to nonaqueous electrolytes," *Chemical Society Reviews,* vol. 43, no. 22, pp. 7746-7786, (2014).

[40]. J. HORIUTI, A. MATSUDA, M. ENYO, and H. KITA, "The mechanism of the hydrogen evolution reaction," in *Electrochemistry*: Elsevier, (1965), pp. 750-779.

[41]. J. Bockris, I. Ammar, and A. Huq, "The mechanism of the hydrogen evolution reaction on platinum, silver and tungsten surfaces in acid solutions," *The Journal of Physical Chemistry,* vol. 61, no. 7, pp. 879-886, (1957).

[42]. X. Xu *et al.*, "A perovskite electrocatalyst for efficient hydrogen evolution reaction," *Advanced Materials,* vol. 28, no. 30, pp. 6442-6448, (2016).

[43]. J. D. Benck, T. R. Hellstern, J. Kibsgaard, P. Chakthranont, and T. F. Jaramillo, "Catalyzing the hydrogen evolution reaction (HER) with molybdenum sulfide nanomaterials," *Acs Catalysis,* vol. 4, no. 11, pp. 3957-3971, (2014).

[44]. R. Parsons, "The rate of electrolytic hydrogen evolution and the heat of adsorption of hydrogen," *Transactions of the Faraday Society,* vol. 54, pp. 1053-1063, (1958).

[45]. S. Trasatti, "Electrocatalysis by oxides—attempt at a unifying approach," *Journal of Electroanalytical Chemistry and Interfacial Electrochemistry,* vol. 111, no. 1, pp. 125-131, (1980).

[46]. S. Trasatti, "Electrocatalysis in the anodic evolution of oxygen and chlorine," *Electrochimica Acta,* vol. 29, no. 11, pp. 1503-1512, (1984).

[47]. B. JO'M, T. Otagawa, and V. Young, "Solid state surface studies of the electrocatalysis of oxygen evolution on perovskites," *Journal of Electroanalytical Chemistry and Interfacial Electrochemistry,* vol. 150, no. 1-2, pp. 633-643, (1983).

[48]. J. O. M. Bockris and T. Otagawa, "Mechanism of oxygen evolution on perovskites," *The Journal of Physical Chemistry,* vol. 87, no. 15, pp. 2960-2971, (2002).

[49]. I. C. Man *et al.,* "Universality in oxygen evolution electrocatalysis on oxide surfaces," *ChemCatChem,* vol. 3, no. 7, pp. 1159-1165, (2011).

[50]. D. A. Kuznetsov *et al.,* "Tuning redox transitions via inductive effect in metal oxides and complexes, and implications in oxygen electrocatalysis," *Joule,* vol. 2, no. 2, pp. 225-244, 2018.

[51]. J. Suntivich, H. A. Gasteiger, N. Yabuuchi, H. Nakanishi, J. B. Goodenough, and Y. Shao-Horn, "Design principles for oxygen-reduction activity on perovskite oxide catalysts for fuel cells and metal–air batteries," *Nature chemistry,* vol. 3, no. 7, pp. 546-550, (2011).

[52]. J. Suntivich, K. J. May, H. A. Gasteiger, J. B. Goodenough, and Y. Shao-Horn, "A perovskite oxide optimized for oxygen evolution catalysis from molecular orbital principles," *Science,* vol. 334, no. 6061, pp. 1383-1385, (2011).

[53]. J. K. Nørskov *et al.,* "Origin of the overpotential for oxygen reduction at a fuel-cell cathode," *The Journal of Physical Chemistry B,* vol. 108, no. 46, pp. 17886-17892, (2004).

[54]. J. Rossmeisl, A. Logadottir, and J. K. Nørskov, "Electrolysis of water on (oxidized) metal surfaces," *Chemical physics,* vol. 319, no. 1-3, pp. 178-184, (2005).

[55]. J. Rossmeisl, Z.-W. Qu, H. Zhu, G.-J. Kroes, and J. K. Nørskov, "Electrolysis of water on oxide surfaces," *Journal of Electroanalytical Chemistry,* vol. 607, no. 1-2, pp. 83-89, (2007).

[56]. Y. Zhu, J. Dai, W. Zhou, Y. Zhong, H. Wang, and Z. Shao, "Synergistically enhanced hydrogen evolution electrocatalysis by in situ exsolution of metallic nanoparticles on perovskites," *Journal of Materials Chemistry A*, vol. 6, no. 28, pp. 13582-13587, (2018).

[57]. J. T. Mefford *et al.*, "Water electrolysis on La1− xSrxCoO3− δ perovskite electrocatalysts," *Nature communications*, vol. 7, no. 1, pp. 1-11, (2016).

[58]. X. Rong, J. Parolin, and A. M. Kolpak, "A fundamental relationship between reaction mechanism and stability in metal oxide catalysts for oxygen evolution," *Acs Catalysis*, vol. 6, no. 2, pp. 1153-1158, (2016).

[59]. S. She, J. Yu, W. Tang, Y. Zhu, Y. Chen, and J. Sunarso, "Ocatalysts in alkaline media a systematic study of oxygen evolution activity and stability on La 1-x Sr x FeO 3-δ perovskite electrocatalysts in alkaline: A systematic study of oxygen evolution activity and stability on La1-XSrxFeO3-# Perovskite Electr med," *Appl Mater Interfaces*, vol. 10, pp. 11715-11721, (2018).

[60]. C. Jin, X. Cao, L. Zhang, C. Zhang, and R. Yang, "Preparation and electrochemical properties of urchin-like La0. 8Sr0. 2MnO3 perovskite oxide as a bifunctional catalyst for oxygen reduction and oxygen evolution reaction," *Journal of power sources*, vol. 241, pp. 225-230, (2013).

[61]. J. Tulloch and S. W. Donne, "Activity of perovskite La1− xSrxMnO3 catalysts towards oxygen reduction in alkaline electrolytes," *Journal of Power Sources*, vol. 188, no. 2, pp. 359-366, (2009).

[62]. Y. Duan *et al.*, "Tailoring the Co 3d-O 2p covalency in LaCoO3 by Fe substitution to promote oxygen evolution reaction," *Chemistry of Materials*, vol. 29, no. 24, pp. 10534-10541, 2017.

[63]. S. Tiwari, S. Singh, and R. Singh, "Effects of Ni, Fe, Cu, and Cr substitutions for Co in La0. 8Sr0. 2CoO3 on electrocatalytic properties for oxygen evolution," *Journal of the Electrochemical Society*, vol. 143, no. 5, p. 1505, (1996).

[64]. K. J. May *et al.*, "Influence of oxygen evolution during water oxidation on the surface of perovskite oxide catalysts," *The journal of physical chemistry letters*, vol. 3, no. 22, pp. 3264-3270, (2012).

[65]. Y.-f. Bu *et al.*, "A high-performance, cobalt-free cathode for intermediate-temperature solid oxide fuel cells with excellent CO2 tolerance," *Journal of Power Sources*, vol. 319, pp. 178-184, (2016).

[66]. Y.-M. Chang, Y.-F. Chang, P.-W. Wu, C.-Y. Wu, and P. Lin, "Synthesis and characterization of La0. 6Ca0. 4Co0. 8Ru0. 2O3 for oxygen reduction reaction in an alkaline electrolyte," *Journal of the Electrochemical Society,* vol. 157, no. 6, p. B900, (2010).

[67]. Y. Shen *et al.*, "New Phosphorus-Doped Perovskite Oxide as an Oxygen Reduction Reaction Electrocatalyst in an Alkaline Solution," *Chemistry–A European Journal,* vol. 24, no. 27, pp. 6950-6957, (2018).

[68]. Y. Zhu, W. Zhou, J. Sunarso, Y. Zhong, and Z. Shao, "Phosphorus-doped perovskite oxide as highly efficient water oxidation electrocatalyst in alkaline solution," *Advanced Functional Materials,* vol. 26, no. 32, pp. 5862-5872, (2016).

[69]. H. Sun, G. Chen, J. Sunarso, J. Dai, W. Zhou, and Z. Shao, "Molybdenum and niobium codoped B-site-ordered double perovskite catalyst for efficient oxygen evolution reaction," *ACS applied materials & interfaces,* vol. 10, no. 20, pp. 16939-16942, (2018).

[70]. X. Xu, Y. Chen, W. Zhou, Y. Zhong, D. Guan, and Z. Shao, "Earth-abundant silicon for facilitating water oxidation over iron-based perovskite electrocatalyst," *Advanced materials interfaces,* vol. 5, no. 11, p. 1701693, (2018).

[71]. Y. Zhu, W. Zhou, J. Yu, Y. Chen, M. Liu, and Z. Shao, "Enhancing electrocatalytic activity of perovskite oxides by tuning cation deficiency for oxygen reduction and evolution reactions," *Chemistry of Materials,* vol. 28, no. 6, pp. 1691-1697, (2016).

[72]. Q. A. Islam, R. Majee, and S. Bhattacharyya, "Bimetallic nanoparticle decorated perovskite oxide for state-of-the-art trifunctional electrocatalysis," *Journal of Materials Chemistry A,* vol. 7, no. 33, pp. 19453-19464, (2019).

[73]. H. Liu, X. Ding, L. Wang, D. Ding, S. Zhang, and G. Yuan, "Cation deficiency design: A simple and efficient strategy for promoting oxygen evolution reaction activity of perovskite electrocatalyst," *Electrochimica Acta,* vol. 259, pp. 1004-1010, (2018).

[74]. M. Yuasa, G. Sakai, K. Shimanoe, Y. Teraoka, and N. Yamazoe, "Reverse Micelle-Based Preparation of Carbon-Supported La1− x Sr x Mn1− y Fe y O 3+ δ for Oxygen Reduction Electrode," *Journal of The Electrochemical Society,* vol. 151, no. 10, p. A1690, (2004).

[75]. R. Singh, J. Singh, and A. Singh, "Electrocatalytic properties of new spinel-type MMoO4 (M= Fe, Co and Ni) electrodes for oxygen evolution in alkaline solutions," *international journal of hydrogen energy*, vol. 33, no. 16, pp. 4260-4264, (2008).

[76]. W. Zhou and J. Sunarso, "Enhancing bi-functional electrocatalytic activity of perovskite by temperature shock: A case study of LaNiO3− δ," *The journal of physical chemistry letters*, vol. 4, no. 17, pp. 2982-2988, (2013).

[77]. J. Du, T. Zhang, F. Cheng, W. Chu, Z. Wu, and J. Chen, "Nonstoichiometric perovskite CaMnO3− δ for oxygen electrocatalysis with high activity," *Inorganic chemistry*, vol. 53, no. 17, pp. 9106-9114, (2014).

[78]. J. Kim, X. Yin, K.-C. Tsao, S. Fang, and H. Yang, "Ca2Mn2O5 as oxygen-deficient perovskite electrocatalyst for oxygen evolution reaction," *Journal of the American Chemical Society*, vol. 136, no. 42, pp. 14646-14649, (2014).

[79]. C.-F. Chen *et al.*, "Oxygen-deficient BaTiO3− x perovskite as an efficient bifunctional oxygen electrocatalyst," *Nano Energy*, vol. 13, pp. 423-432, (2015).

[80]. Z. Wang *et al.*, "Nickel-Doped La0. 8Sr0. 2Mn1–x Ni x O3 Nanoparticles Containing Abundant Oxygen Vacancies as an Optimized Bifunctional Catalyst for Oxygen Cathode in Rechargeable Lithium–Air Batteries," *ACS applied materials & interfaces*, vol. 8, no. 10, pp. 6520-6528, (2016).

[81]. J. M. Christ *et al.*, "Synthesis of high surface area Ca x La (1− x) Al (1− x) Mn x O (3− δ) perovskite oxides for oxygen reduction electrocatalysis in alkaline media," *Catalysis Science & Technology*, vol. 6, no. 21, pp. 7744-7751, (2016).

[82]. B.-Q. Li, Z.-J. Xia, B. Zhang, C. Tang, H.-F. Wang, and Q. Zhang, "Regulating p-block metals in perovskite nanodots for efficient electrocatalytic water oxidation," *Nature communications*, vol. 8, no. 1, pp. 1-7, (2017).

[83]. G. Chen *et al.*, "An amorphous nickel–iron-based electrocatalyst with unusual local structures for ultrafast oxygen evolution reaction," *Advanced Materials*, vol. 31, no. 28, p. 1900883, (2019).

[84]. Y. Zhu *et al.*, "Unusual synergistic effect in layered Ruddlesden− Popper oxide enables ultrafast hydrogen evolution," *Nature communications*, vol. 10, no. 1, pp. 1-9, (2019).

[85]. Y. Zhu *et al.*, "A perovskite nanorod as bifunctional electrocatalyst for overall water splitting," *Advanced Energy Materials*, vol. 7, no. 8, p. 1602122, (2017).

[86]. F. Deganello *et al.*, "Perovskite-Type Catalysts Prepared by Nanocasting: Effect of Metal Silicates on the Electrocatalytic Activity toward Oxygen Evolution and Reduction Reactions," *ACS Applied Energy Materials,* vol. 1, no. 6, pp. 2565-2575, (2018).

[87]. H. Sun *et al.*, "Boosting the oxygen evolution reaction activity of a perovskite through introducing multi-element synergy and building an ordered structure," *Journal of Materials Chemistry A,* vol. 7, no. 16, pp. 9924-9932, (2019).

[88]. H. Sun, G. Chen, Y. Zhu, B. Liu, W. Zhou, and Z. Shao, "B-site cation ordered double perovskites as efficient and stable electrocatalysts for oxygen evolution reaction," *Chemistry–A European Journal,* vol. 23, no. 24, pp. 5722-5728, (2017).

[89]. N.-I. Kim *et al.*, "Oxygen-deficient triple perovskites as highly active and durable bifunctional electrocatalysts for oxygen electrode reactions," *Science advances,* vol. 4, no. 6, p. eaap9360, 2018.

[90]. J. Wang *et al.*, "Water splitting with an enhanced bifunctional double perovskite," *ACS catalysis,* vol. 8, no. 1, pp. 364-371, (2018).

[91] K. J. Stevenson *et al.*, "Highly Active, Nonprecious Metal Perovskite Electrocatalysts for Bifunctional Metal-Air Battery Electrodes," in *ECS Meeting Abstracts*, (2013), no. 4: IOP Publishing, p. 233.

[92]. J. Kim, X. Chen, P.-C. Shih, and H. Yang, "Porous perovskite-type lanthanum cobaltite as electrocatalysts toward oxygen evolution reaction," *ACS Sustainable Chemistry & Engineering*, vol. 5, no. 11, pp. 10910-10917, (2017).

[93]. S. Tiwari, P. Chartier, and R. Singh, "Preparation of Perovskite-Type Oxides of Cobalt by the Malic Acid Aided Process and Their Electrocatalytic Surface Properties in Relation to Oxygen Evolution," *Journal of The Electrochemical Society,* vol. 142, no. 1, p. 148, (1995).

[94]. M. Yuasa, N. Tachibana, and K. Shimanoe, "Oxygen Reduction Activity of Carbon-Supported La1–x Ca x Mn1–y Fe y O3 Nanoparticles," *Chemistry of Materials,* vol. 25, no. 15, pp. 3072-3079, (2013).

[95]. Y.-M. Chang, Y.-C. Hsieh, P.-W. Wu, C.-H. Lai, and T.-Y. Chang, "Enhancement of bifunctional catalysis by Ir doping of La0. 6Ca0. 4CoO3 perovskites," *Materials Letters,* vol. 62, no. 26, pp. 4220-4222, (2008).

[96]. S. Park, E.-K. Lee, H. Song, and Y.-T. Kim, "Bifunctional enhancement of oxygen reduction reaction activity on Ag catalysts due to water activation on

LaMnO3 supports in alkaline media," *Scientific reports*, vol. 5, no. 1, pp. 1-14, (2015).

[97]. C. Soares, M. Carvalho, A. Tavares, M. M. Jorge, A. Gomes, and M. da Silva Pereira, "PtRu/C-LaNiO3 composite electrodes for electrocatalysis," *Journal of The Electrochemical Society*, vol. 160, no. 10, p. F1138, (2013).

[98]. X. Han, F. Cheng, T. Zhang, J. Yang, Y. Hu, and J. Chen, "Hydrogenated uniform Pt clusters supported on porous CaMnO3 as a bifunctional electrocatalyst for enhanced oxygen reduction and evolution," *Advanced Materials*, vol. 26, no. 13, pp. 2047-2051, (2014).

[99]. T. D. Thanh, N. D. Chuong, J. Balamurugan, H. Van Hien, N. H. Kim, and J. H. Lee, "Porous Hollow-Structured LaNiO3 Stabilized N, S-Codoped Graphene as an Active Electrocatalyst for Oxygen Reduction Reaction," *Small*, vol. 13, no. 39, p. 1701884, (2017).

[100]. Y. Bu *et al.*, "Synergistic interaction of perovskite oxides and N-doped graphene in versatile electrocatalyst," *Journal of Materials Chemistry A*, vol. 7, no. 5, pp. 2048-2054, (2019).

[101]. J. Mathias, "How does FTIR work_ _ _ Innovatech labs," (2015).

[102]. J. M. Thomas, " "heterogeneous catalysis". Wiley-VCH

(2015).

[103.] P. T. K. a. W. R. Heineman, "Cyclic voltammetry," *Journal of Chemical Education*, vol. 60, pp. 702-706, (1983).

[104]. C. S. a. J. M. Gohil, "Microbial desalination cell technology:Functions and Future Prospects," *Elsevier*, pp. 399-422, (2018).

[105]. J. Xu, X. Zhou, X. Dong, L. Pan, and K. Sun, "Catalytic activity of infiltrated La0. 3Sr0. 7Ti0. 3Fe0. 7O3− δ–CeO2 as a composite SOFC anode material for H2 and CO oxidation," *International Journal of Hydrogen Energy*, vol. 42, no. 23, pp. 15632-15640, (2017).

[106]. S. R. Yashas *et al.*, "Sonochemical synthesis of graphitic carbon nitride-manganese oxide interfaces for enhanced photocatalytic degradation of tetracycline hydrochloride," *Environmental Science and Pollution Research*, vol. 28, no. 4, pp. 4778-4789, (2021).

[107]. R. Khan *et al.*, "A highly efficient A-site deficient perovskite interlaced within two dimensional MXene nanosheets as an active electrocatalyst for hydrogen production," (2021).

[108]. Y. Zhu, J. Dai, W. Zhou, Y. Zhong, H. Wang, and Z. J. J. o. M. C. A. Shao, "Synergistically enhanced hydrogen evolution electrocatalysis by in situ exsolution of metallic nanoparticles on perovskites," vol. 6, no. 28, pp. 13582-13587, (2018).

[109]. D. P. Dubal, G. S. Gund, C. D. Lokhande, R. J. A. a. m. Holze, and interfaces, "Decoration of spongelike Ni (OH) 2 nanoparticles onto MWCNTs using an easily manipulated chemical protocol for supercapacitors," vol. 5, no. 7, pp. 2446-2454, (2013).

[110]. D. L. Keshebo *et al.*, "Effect of composition of few-layered transition metal dichalcogenide nanosheets on separation mechanism of hydrogen selective membranes," vol. 634, p. 119419, (2021).

[111]. J. Liu *et al.*, "Hierarchical NiCo2S4@ NiFe LDH heterostructures supported on nickel foam for enhanced overall-water-splitting activity," vol. 9, no. 18, pp. 15364-15372, (2017).

[112]. F. Yusoff, N. Mohamed, A. Aziz, S. J. M. S. Ab Ghani, and Applications, "Electrocatalytic reduction of oxygen at perovskite (BSCF)-MWCNT composite electrodes," vol. 2014, (2014).

[113]. N. Shuhaimi, L. Teo, H. Woo, S. R. Majid, and A. K. J. P. b. Arof, "Electrical double-layer capacitors with plasticized polymer electrolyte based on methyl cellulose," vol. 69, no. 7, pp. 807-826, (2012).

[114]. Y.-P. Gao, K.-J. Huang, X. Wu, Z.-Q. Hou, Y.-Y. J. J. o. a. Liu, and compounds, "MoS2 nanosheets assembling three-dimensional nanospheres for enhanced-performance supercapacitor," vol. 741, pp. 174-181, (2018).

[115]. X. Zhang *et al.*, "Synergistic effects of lanthanum and strontium to enhance the osteogenic activity of TiO2 nanotube biological interface," vol. 46, no. 9, pp. 13969-13979, (2020).

[116]. M. Risch *et al.*, "Structural changes of cobalt-based perovskites upon water oxidation investigated by EXAFS," *The Journal of Physical Chemistry C,* vol. 117, no. 17, pp. 8628-8635, (2013).